JGR Atmospheres

RESEARCH ARTICLE
10.1029/2019JD031989

# Land Cover Impacts on Land-Atmosphere Coupling Strength in Climate Simulations With WRF Over Europe

**Lisa Jach[1], Kirsten Warrach-Sagi[1], Joachim Ingwersen[2], Eigil Kaas[3], and Volker Wulfmeyer[1]**

[1]Institute for Physics and Meteorology, University of Hohenheim, Stuttgart, Germany, [2]Institute for Soil Science and Land Evaluation, Department of Biogeophysics, University of Hohenheim, Stuttgart, Germany, [3]Niels Bohr Institute, Department of Climate and Computational Geophysics, University of Copenhagen, Copenhagen, Denmark

**Key Points:**
- A region of strong coupling was identified in the northeast of Europe, and the location was not shifted by land use and land cover changes
- Land-atmosphere feedbacks appear to be mainly positive in Europe, and extreme afforestation and deforestation modify the coupling strength
- Significant impacts on clouds and precipitation occur over mountains and the coupling hot spot; however, the impacts are rather limited

**Supporting Information:**
- Supporting Information S1

**Correspondence to:**
L. Jach,
lisa.jach@uni-hohenheim.de

**Citation:**
Jach, L., Warrach-Sagi, K., Ingwersen, J., Kaas, E., & Wulfmeyer, V. (2020). Land cover impacts on land-atmosphere coupling strength in climate simulations with WRF over Europe. *Journal of Geophysical Research: Atmospheres*, *125*, e2019JD031989. https://doi.org/10.1029/2019JD031989

Received 6 NOV 2019
Accepted 19 AUG 2020
Accepted article online 31 AUG 2020



**Abstract** Land use and land cover changes are important human forcings to the Earth's climate. This study examines the land-atmosphere coupling strength and the relationship between surface fluxes and clouds and precipitation for three land cover scenarios in the European summer. The WRF model was used to simulate one scenario with extreme afforestation, one with extreme deforestation, and one with realistic land cover for the time period between 1986 and 2015. The simulations were forced with ERA-Interim reanalysis data. The analysis followed a two-step approach. First, the convective triggering potential–low-level humidity index framework was applied to locate potential coupling hot spots, which were then analyzed with regard to their sensitivity toward land use and land cover changes. Second, actual feedbacks between evaporative fraction, cloud cover, and precipitation were analyzed statistically with focus on sign and location of the feedbacks. The results demonstrate that coupling hot spots, exhibiting predominantly positive feedbacks, were identified over parts of Eastern Europe and Scandinavia. In this strongly coupled region, afforestation and deforestation modified the atmospheric humidity and stability by changing the surface flux partitioning. Afforestation is associated with a net drying of the atmosphere due to a disproportionately strong increase in the sensible heat flux. In contrast, deforestation initiated a moistening of the atmosphere. The total precipitation changed only in limited areas significantly, which are mostly located in mountainous regions and the northeast of the domain. In summary, the results indicate a land surface influence on the atmospheric background conditions, and an impact on the potential strength of land surface-precipitation feedbacks.

## 1. Introduction

Land-atmosphere (L-A) interactions are key processes in the Earth's climate system. Feedbacks are manifold and strongly interconnected. Thus, modifications on the land surface due to land use and land cover changes (LULCCs) can impact the climate significantly. They affect biogeochemical cycles like carbon storages as well as energy and water fluxes at the land surface (Intergovernmental Panel on Climate Change, 2014, 2019). Variations in the latter appear due to modifications in biogeophysical properties of the land surface such as albedo, roughness length, leaf area index, or stomatal resistance.

Underestimating biogeophysical forcings to the climate in models may lead to significant biases in a number of variables. de Noblet-Ducoudré et al. (2012) find that the regional biogeophysical impacts of LULCC can exceed the magnitude of radiative forcing caused by greenhouse gas emissions, although their assessment is still uncertain in sign and magnitude within climate models (Davin & de Noblet-Ducoudré, 2010). This is because counteracting effects of radiative and nonradiative processes on water and energy exchanges vary in time and space and depend on the type of LULCC (Duveiller, Forzieri, et al., 2018; Duveiller, Hooker, & Cescatti, 2018; Snyder et al., 2004). Deforestation, for example, increases the surface albedo, because cropland or grassland usually have a brighter surface than forests. The resulting loss in available energy cools the surface. The concurrent decrease in leaf area and stomatal resistance reduces transpiration, which leads to a reduction of evaporative cooling and, hence, to a warming. The net effect depends on which of these processes dominates (Davin & de Noblet-Ducoudré, 2010). Different forest types diverge in their biogeophysical and biogeochemical forcings, too. Transitions of boreal forests have the largest biogeophysical effects of all

vegetation types as they have a lower summertime evaporative fraction (EF) than other forests. Their lower albedo increases the available energy at the surface. The additional energy is partitioned into sensible rather than latent heat (Baldocchi et al., 2000; Bonan, 2008; Snyder et al., 2004). Studies of global climate-vegetation dynamics reveal a significant impact of vegetation on the climate and vice versa (e.g., Kumar et al., 2013). Thus, LULCCs have recently become the focus of studies aiming to assess their role in past temperature trends (e.g., Boisier et al., 2012; Huang et al., 2020; Pitman et al., 2009), extreme events (e.g., Findell et al., 2017; Hirsch et al., 2015), and modification of precipitation patterns (e.g., Bagley et al., 2014; Chen et al., 2017; Chen & Dirmeyer, 2017; Lawrence & Chase, 2010). Mahmood et al. (2014) provide an overview of the most notable LULCC and their effects on the climate, and Snyder et al. (2004) assess the influence of vegetation biomes on the climate.

The L-A coupling strength is an approach to quantify the relationship between the land surface and atmospheric states and fluxes. The coupling strength is subject to regional variability (Findell & Eltahir, 2003b; Koster et al., 2004) and temporal variability (Dirmeyer et al., 2014; Guo & Dirmeyer, 2013; Seneviratne et al., 2006), which raises the question of which factors determine the strength of L-A coupling. The lack of a common definition along with the fact that different studies and metrics address different quantities and processes (Knist et al., 2017) complicates the comparability of studies on L-A coupling strength. Additionally, disparate atmospheric models and resolutions, high land surface complexity, and lack of observations make assessments difficult as well (Santanello et al., 2009). Furthermore, many studies have been performed on a global scale and on rather coarse resolutions. Koster et al. (2004), for example, examine the soil moisture-precipitation coupling using an ensemble of atmospheric general circulation models. They find a weak coupling hot spot in Eastern Europe. However, studies on the continental scale are still rare for Europe. Knist et al. (2017) investigate the coupling between soil moisture and surface fluxes as well as surface fluxes and near-surface air temperature variations. They locate a coupling hot spot in eastern-central Europe and attribute this link to reduced or missing dominant moisture or energy limitations on evapotranspiration. Only a limited number of L-A observational studies are currently available, for example, the Land Atmosphere Feedback Experiment (LAFE; Wulfmeyer et al., 2018, 2020). Therefore, new observations dedicated to measuring L-A interactions are under development in Europe. One example is the Land Atmosphere Feedback Observatory (LAFO; https://lafo.uni-hohenheim.de/, Späth et al. (2019).

Until now, few studies have employed regional climate models (RCMs) to investigate LULCC forcings on the climate in Europe (Cherubini et al., 2018; Davin et al., 2014; Tölle et al., 2014). The studies usually apply static land cover maps to investigate biogeophysical impacts of single LULCC such as afforestation (e.g., Gálos et al., 2013; Gao et al., 2014). However, realistic, transient LULCCs have not been included in previous RCM-intercomparison studies in Europe (e.g., Christensen & Christensen, 2007). In 2017, the World Climate Research Program Flagship Pilot Study "Land-Use and Climate Across Scales" (LUCAS) was endorsed to investigate the effects of implementing LULCC in RCMs in a coordinated initiative. LUCAS is part of the European branch of the Coordinated Regional Climate Downscaling Experiment (CORDEX, https://www.cordex.org/; Giorgi et al. 2009; Gutowski et al. 2016). They aim at examining biogeophysical impacts and their influence on the regional climate on different spatial and temporal scales. The overarching goal is to investigate the potential of the land surface to mitigate climate change and to provide an improved basis for regional climate impact assessments (Rechid et al., 2017). In LUCAS phase I, three land cover scenarios are implemented in an ensemble of RCMs to compare the impacts of (1) extreme afforestation (FOREST) and (2) extreme deforestation (GRASS) with a (3) realistic land cover (CORINE) as baseline in Europe. In the following presented experiments, afforestation refers to a conversion from all nonforest vegetation types to forest. Deforestation refers to the conversion from all vegetation types to grassland in the respective model run.

This study provides an analysis of WRF-NoahMP simulations made by the University of Hohenheim which were included as part of the LUCAS ensemble (Davin et al., 2020). It is a test bed for future coupling strength studies on the LUCAS-ensemble investigating the effects of realistic LULCC. Simulation experiments with idealized extreme LULCC are well suited for assessing the potential sensitivity of atmospheric responses to land surface modifications. The first objective is to locate long-term mean coupling hot spots between surface fluxes and precipitation based on the early-morning atmospheric structure (Findell & Eltahir, 2003a, 2003b) for the European summer. The coupling hot spots and the coupling strength are then analyzed with

**Table 1**
*Choice of Parameterization Schemes of the WRF Configuration*

| Model physics | Parameterization scheme |
|---|---|
| Microphysics Scheme | New Thompson scheme (Thompson et al., 2004) |
| Short-Wave Radiation Scheme | Rapid Radiative Transfer Model (RRTMG) scheme (Iacono et al., 2008) |
| Long-Wave Radiation Scheme | Rapid Radiative Transfer Model (RRTMG) scheme (Iacono et al., 2008) |
| Boundary Layer Scheme | MYNN Level 2.5 PBL (Nakanishi & Niino, 2009) |
| Convection Scheme | Kain-Fritsch scheme (Kain, 2004) |
| Land Surface Model | NOAH-MP land surface model (Niu et al., 2011) |
| Surface Layer Scheme | MYNN surface layer scheme (Nakanishi & Niino, 2009) |

regard to their sensitivity to extreme LULCC. The second objective is to investigate the relationship between the surface fluxes and clouds and precipitation patterns in dependence of land cover. This work is structured as follows: Section 2 outlines the Materials and Methods, including a model description, the simulation set-up, the land cover scenarios, and the analysis metrics. Section 3 presents the results on L-A coupling strength. Section 4 reports the results on the statistical analysis of the link between surface fluxes, clouds, and total precipitation. The results are discussed in section 5 and summarized in section 6.

## 2. Experimental Design and Methods

### 2.1. Model Description

The RCM used in this study is WRF V3.8.1 (Skamarock et al., 2008) coupled to the Noah land surface model with multiparameterization options (NoahMP) (Niu et al., 2011). For the planetary boundary layer (PBL), the MYNN level 2.5 local turbulence parameterization scheme was applied (Nakanishi & Niino, 2009). In line with the WRFb-CLM configuration of the LUCAS ensemble, the number of vertical levels was set to 40 and the model top to a pressure height of 50 hPa (Davin et al., 2020). The cumulus parameterization followed the approach of Kain (2004). Additional parameterization schemes are listed in Table 1. The final physics configuration was based on previous studies from the authors and others (e.g., see Bauer et al., 2015; Kotlarski et al., 2014; Schwitalla et al., 2017; Warrach-Sagi et al., 2013). Soil moisture was initialized on the 1 January 1984 from ERA-Interim reanalysis data (Dee et al., 2011), and the soil texture was derived from a modified version of the Harmonized World Soil Database (HWSD) (Milovac et al., 2014). The vegetation in each grid cell was considered using a dominant approach, and each land cover type was parameterized after the IGBP-MODIS 21-category land use classification used in WRF. The vegetation dynamics were treated through daily interpolation of monthly leaf area index (LAI) values from the MODIS vegetation parameter table. The calculation of stomatal resistance was performed using the Ball-Berry scheme in combination with green vegetation fraction calculated from LAI and the stem area index.

### 2.2. Simulation Set-Up

Three experiments, which differ in the applied land cover maps, were forced with 6-hourly ERA-Interim reanalysis data on 0.75° resolution from the European Centre for Medium-Range Weather Forecasts. They ran for the years 1984–2015 including 2 years of spin-up, which were excluded from the analyses. All experiments were carried out for the CORDEX domain of Europe (EURO-CORDEX; Jacob et al., 2020) on 0.44° grid spacing. The analyses focused on the summer months of June–August because the sensitivity of convection to land surface influences is expected to be greatest in summer (Dirmeyer et al., 2013; Taylor et al., 2012). Some analyses were carried out for the PRUDENCE subregions (Alps, British Isles, Eastern Europe, France, Iberian Peninsula, Mediterranean, Mid-Europe, and Scandinavia (Christensen & Christensen, 2007). The original subregions were expanded by two additional ones covering the northeastern and eastern parts of the study domain. The Eastern European Plain extends from 44°N to 70°N and 30°E to the eastern border of the domain (Figure 1c). The Black Sea extends from 25°N to 44°N and 36°E to the eastern border of the domain. The range of climate zones in the domain is heterogeneous. According to the Köppen-Geiger classification (Peel et al., 2007), climates vary from cool continental climates with arctic influence in the high latitudes to Mediterranean climate in southern Europe and from oceanic climate in coastal areas to warm, humid continental climate in Eastern Europe. This variety makes L-A feedback studies quite challenging over Europe.

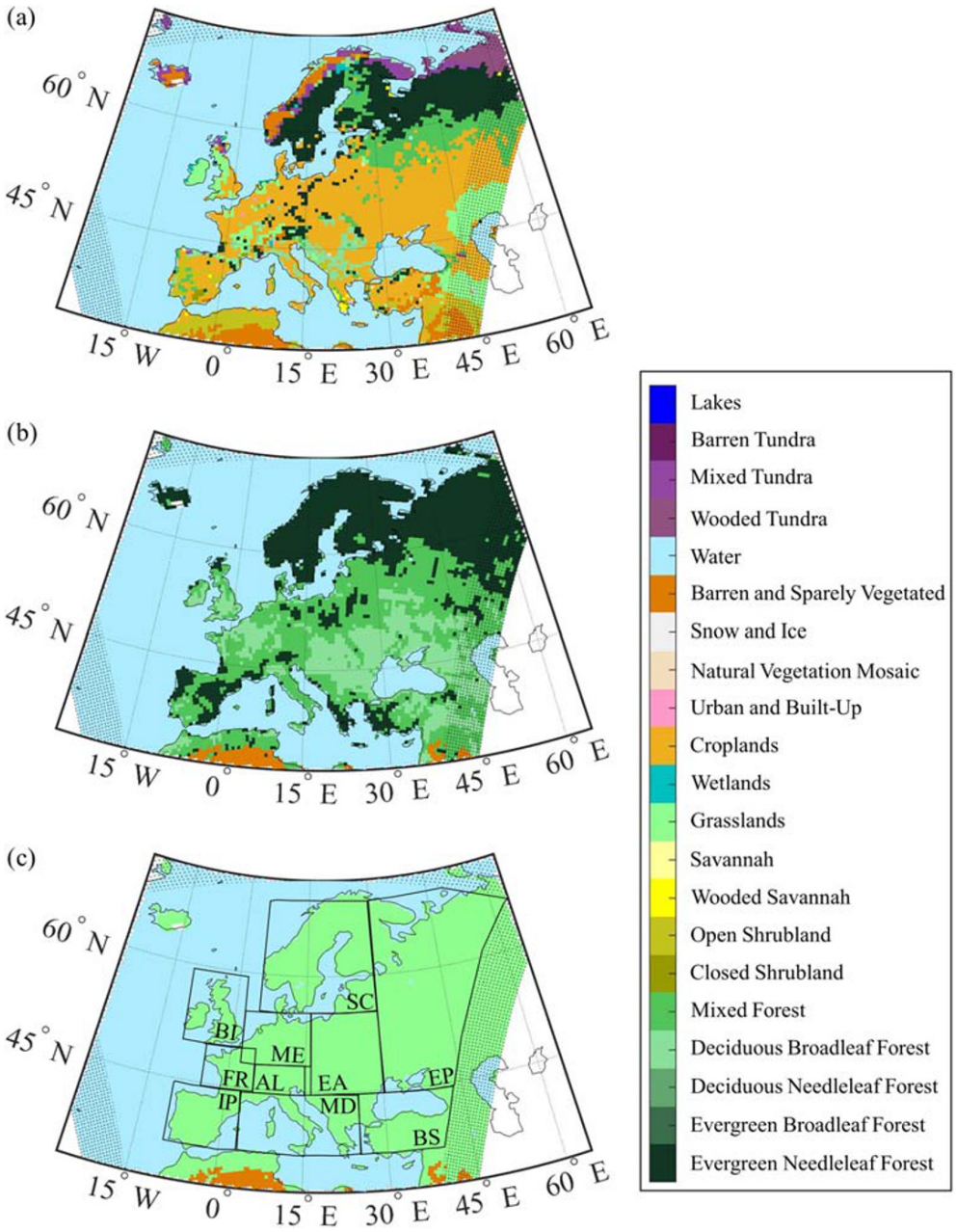


**Figure 1.** Land use maps of (a) the CORINE, (b) the FOREST, and (c) the GRASS experiments in the EURO-CORDEX EUR-44 domain derived from IGBP-MODIS 21-category land use type classification used in the WRF model. Subplot (c) also contains the boundaries of the expanded PRUDENCE-regions: The Alps (AL), British Isles (BI), Black Sea (BS), Eastern Europe (EA), Eastern European Plain (EP), France (FR), Iberian Peninsula (IP), Mediterranean (MD), Mid-Europe (ME), and Scandinavia (SC).

### 2.3. Land Cover Scenarios

L-A feedbacks were investigated for three land covers: (1) a realistic real land cover as baseline (CORINE), (2) maximum forest coverage (FOREST), and (3) maximum grassland coverage (GRASS) in Europe. The CORINE 2006 land cover classification (European Environmental Agency, 2013) was implemented for the baseline run (Figure 1a). In the FOREST scenario, a land cover map was used where the total land area is covered by forest where it can realistically grow. This means areas with cold and hot deserts were not covered with vegetation, as it would be biologically implausible. Similarly, all vegetation types were converted to grassland in the GRASS scenario (see Davin et al., 2020, for a detailed description of the maps).

The land cover maps for the FOREST and GRASS experiments were based on a global MODIS-based present-day land cover map at 0.5° resolution with 17 plant functional types (Lawrence & Chase, 2007). Shrub, crop, and grassland types were set to zero in order to produce the FOREST map. The sum of the remaining forest classes was designed to be 100% excluding nonvegetated areas. The proportion of the individual classes was conserved from the original map. Therefore, needleleaf forests mainly cover the high-latitudes and broadleaf forests grow further to the South. The forest plant functional types were converted to C3 and C4 grassland to derive the grass map. Again, the proportion of each type was taken from the original map. The fraction of bare soil was conserved in both experiments (Davin et al., 2020).

The implementation of the derived maps in WRF-NoahMP required a transfer of the plant functional types to the IGBP-MODIS 21-category land use type classification. Plant functional types that are only differing in the climate as well as C3 and C4 grasses were merged. The IGBP-MODIS classification neither represents climates (tropical or temperate forests) nor diverse grassland types (C3 or C4 grasses). In the forest map, cells were classified as Mixed Forests when they had a similar share of different forest types. Finally, cells classified as Ice and Snow in the CORINE 2006 land cover classification were used to mask both the forest and the grass map (Figures 1b and 1c). In the following, afforestation denotes the comparison FOREST-CORINE and deforestation the comparison GRASS-CORINE.

### 2.4. Land-Atmosphere Coupling Metrics

#### 2.4.1. CTP-$HI_{low}$ Framework

In the past decade, different studies suggested that among other things, the atmospheric conditions in the early morning influence whether the land surface may impact convection triggering throughout the day. While some atmospheric conditions favor convection initiation by increasing the atmospheric moisture (positive feedbacks) (Guillod et al., 2015; Koster et al., 2004), others favor convection initiation by increasing the boundary layer growth through high sensible heat fluxes (negative feedbacks) (Dirmeyer et al., 2014; Taylor et al., 2012). Different regions exhibit a different dominant feedback sign in dependence of the prevailing atmospheric conditions (Findell et al., 2011). The convective triggering potential (CTP)-low-level humidity index ($HI_{low}$) framework (Findell & Eltahir, 2003a, 2003b) evaluates the potential for the triggering of deep convection in dependence of land surface forcing. It uses the stability and the humidity deficit of the residual layer around the hour of sunrise for this (Dione et al., 2014). It is composed of two atmospheric properties. The CTP is the departure of the modeled temperature profile from the moist adiabatic lapse rate between 100 and 300 hPa above ground. The $HI_{low}$ is the sum of dew-point depressions at 50 and 150 hPa above ground. The variables are fully defined in the Appendix. Further details on data processing are given there, too.

At first, CTP and $HI_{low}$ are used to assess the type of early-morning profile within the CTP-$HI_{low}$ space on each day for every cell (Figure 2a). The threshold values from Findell and Eltahir (2003a) are used to distinguish between days with a wet soil advantage favoring positive feedbacks (1), days with a dry soil advantage favoring negative feedbacks (2), days in a transition zone (3), and atmospherically controlled (AC) days (4). On days with AC conditions, an influence of the surface fluxes on convective precipitation is unlikely. Days are considered AC in three cases. Negative CTP values indicate a temperature inversion in the early-morning atmosphere, which inhibits deep convection. When the humidity deficit is very high ($HI_{low} > 15$°C), precipitation is generally unlikely, and when the humidity deficit is very low ($HI_{low} < 5$°C), precipitation is likely over any surface (Findell & Eltahir, 2003b). Days in the feedback categories (categories 1–3) are jointly referred to as nonatmospherically controlled (nAC) days. The quantity gives an idea of how frequently the land surface may impact convection triggering. The distinction of the different feedback categories enables the assessment of the predominant feedback sign. An atmosphere with a humidity deficit between 5°C and 10°C and unstable conditions (CTP > 0 J/kg) is associated with a wet soil advantage (Figure 2a). Dryer conditions in the atmosphere (10 °C < $HI_{low}$ < 15°C) and high instability (CTP > 200 J/kg) suggest a dry soil advantage (Figure 2a). In the transition zone (Figure 2a), wet or dry soils can both be advantageous. These days are characterized by lower humidity conditions (10°C < $HI_{low}$ < 15°C) and low instability (50 J/kg < CTP < 200 J/kg).

In a second step, the relative occurrence of each type of sounding is quantified to evaluate the potential for land surface effects on convection triggering. When a high potential is apparent, the dominant feedback sign is determined for the chosen period (Figure 2b). Each land grid point is classified either as AC, wet

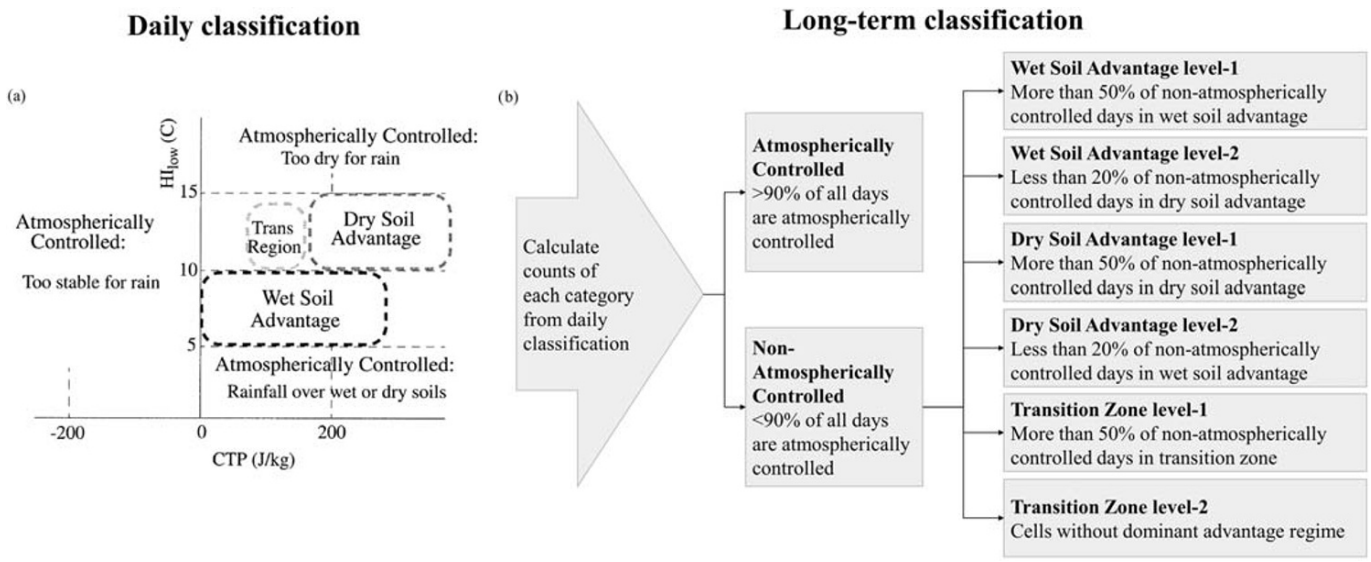


**Figure 2.** (a) Schematic of the CTP-$HI_{low}$ framework adapted from Findell and Eltahir (2003a) their Figure 15 showing the respective profile types in CTP-$HI_{low}$ space. (b) The long-term classification of a cell is based on the relative frequency of occurrence of each class from (a) in a cell. The schematic displays the descriptions of long-term labeling explained in Findell and Eltahir (2003b).

soil advantage, dry soil advantage, or transition zone with their respective subdivisions (Figure 2b). Furthermore, subcategories of AC are included which indicate the major reason for classifying a cell as AC. AC dry, for example, denotes that $HI_{low}$ is larger than 15°C in the majority of days. Levels 1 and 2 denote the strength of the signal within the feedback categories. The labeling as wet soil advantage level 1 signifies a strong positive signal. This label requires that at least 50% of the nAC days are in wet soil advantage. The same applies for the labeling as transition zone level 1 or dry soil advantage level 1. A cell labeled with level 2 has likely a weaker signal. The labeling as wet soil advantage level 2 requires that less than 20% of the nAC days are in dry soil advantage. For the label dry soil advantage level 2, less than 20% of a cell's nAC days are in wet soil advantage. The label transition zone level 2 includes all remaining cells.

The threshold for determining whether a cell is AC or nAC was lowered from originally 20% to 10% (Figure 2b). A review of the frequency of large-scale weather patterns associated with high potential for convective precipitation events in Europe showed that these occur in about 10% of the summer days (Dittmann & Deutscher Wetterdienst, 1995; Lang, 2010). Local convective precipitation events in summer may cause severe damages and floods also in Central Europe. Therefore, it is of social and economic interest to represent potential feedbacks that could impact these events. Testing threshold values between 5% and 30% showed that the choice of the value only affected the size of the region considered as feedback region. The fraction of nAC days and the prevailing advantage for wet/dry soils within a cell was not affected (not shown).

### 2.4.2. Statistics on Land-Atmosphere Feedbacks

Statistical analyses were used to explore the relationship between EF, clouds, and total precipitation with diverging land cover. Due to the model grid increment (0.44°), the model data did not permit a reasonable distinction of convective and synoptic clouds and precipitation. The link between EF [latent heat flux/ (sensible + latent heat flux)] and total precipitation, as well as $HI_{low}$ and total precipitation were further explored on the basis of statistical analyses. Daily mean EF, daily early-morning $HI_{low}$, and daily total precipitation were used for these analyses. Please note that LULCCs are expected also to affect the relationship between soil moisture and EF. This relationship and the influence of EF on precipitation would need to be disentangled. Therefore, EF was used to represent the land surface rather than soil moisture. The cloud statistics in section 4.1 are based on 3-hourly cloud fractions. The significance of differences between the experiments was tested using a Student's *t* test applying a significance level of 5%.

The dependence of precipitation on either EF or $HI_{low}$ was examined by calculating a regression coefficient and multiplying it by the standard deviation of the respective variable. Combining the regression coefficient as a sensitivity measure with the standard deviation as a variability measure follows the reasoning of the

two-legged metric by Dirmeyer (2011). The coefficients of determination of the regressions were investigated to estimate the share of the variance in precipitation that can be explained by EF or $HI_{low}$ dynamics, respectively.

The probability for precipitation (precipitation >1 mm) was compared for AC and nAC days. The probability for precipitation was calculated for each bin by first fitting a probability density function for a Gamma distribution. Second, the area under the function was integrated to approximate the probability of precipitation. As the chosen interval size equals 1, the probability density is an approximation for the probability for the chosen interval. Furthermore, the probability for precipitation was analyzed for different ranges of EF. For this purpose, the summer days were subdivided in four equal bins according to their prevailing EF: (1) EF between 0 and 0.25, (2) EF between 0.25 and 0.5, (3) EF between 0.5 and 0.75, and (4) EF between 0.75 and 1 before calculating the probability. The control group contains the total range of EF.

## 3. Land-Atmosphere Coupling Strength Analysis

### 3.1. Coupling Hot Spots

The CTP-$HI_{low}$ framework was used to identify potential hot spots for surface moisture-precipitation feedbacks and to determine their dominant sign in Europe. The highest potential for a surface impact on deep convection triggering was found in the northeast of the study area (Figure 3, areas in green or orange), where continental climate prevails (Peel et al., 2007). Typically, continental climate is characterized by pronounced variability in weather patterns because of the missing dampening effect of oceans (Bonan, 2016). Figure 4 displays the components of the CTP-$HI_{low}$ framework. Atmospheric conditions were frequently weakly unstable and intermediately humid (Figures 4a and 4d) in the Northeast. This led to a potential nAC in up to 42.2% (CORINE, Figure 4g) of the summer days over the Eastern European Plain (FOREST: 37.2% and GRASS: 37.8%; not shown).

Feedbacks were predominantly positive in the strong coupling region in each experiment. The share of wet soil advantage days in summer was particularly high in the high-latitudes and decreased southward (Figure S2 in the supporting information). The shares of transition zone and dry soil advantage days both increased toward the south, which was due to a higher humidity deficit and, in case of the dry soil advantage days, higher instability in the residual layer. Dry soil advantage days represented the lowest share all over the domain. The north-south gradient in the frequency distribution of the feedback categories appeared independently of the land cover (Figures S1 and S2).

In southern Europe and at the Atlantic coast, the summer days were almost entirely AC (Figures 3 and 4g) in all experiments. Over the British Isles and at the Scandinavian coast, most early-morning soundings were stable (CTP < 0 J $kg^{-1}$) and rather humid ($HI_{low}$ < 5°C) (Figures 4a and 4d). This indicated that convection was regularly inhibited by a stable layer, and the surface fluxes hardly initiated any precipitation event (Findell & Eltahir, 2003a; van den Hurk & van Meijgaard, 2010). Summers were typically dry in southern and southwestern Europe, because the subtropical high extends to up to 40°N. Therefore, the probability for precipitation was low, and along with that, the humidity deficit was on average too large to permit a land surface impact on precipitation (Figure 4d). In other words, the moisture flux into the atmosphere was too small to produce clouds and develop precipitation locally. Findell and Eltahir (2003b) applied similar reasoning within their explanations of atmospheric controls in the United States. Similar to the European high latitudes, soundings at the northwestern US Pacific coast were almost entirely stable and humid, while soundings at the southwestern Pacific coast were very dry. The reasoning for atmospheric controls was valid in all experiments, and the location of potentially strong feedbacks appeared rather insensitive to LULCC (Figure 3). The robustness of the location was further tested by perturbing the initial temperature and moisture profiles before classifying the feedback regions (see supporting information). A shift to a completely different region only occurred with extreme and unrealistic moisture increases combined with considerable decreases in temperature (Figure S4).

### 3.2. Land Surface Impact on Coupling Strength

Although the location of the potential coupling hot spot appeared to be robust, modifications of the surface flux partitioning could influence the local L-A coupling strength (Figures 4h and 4i) and the predominance of the feedback sign.

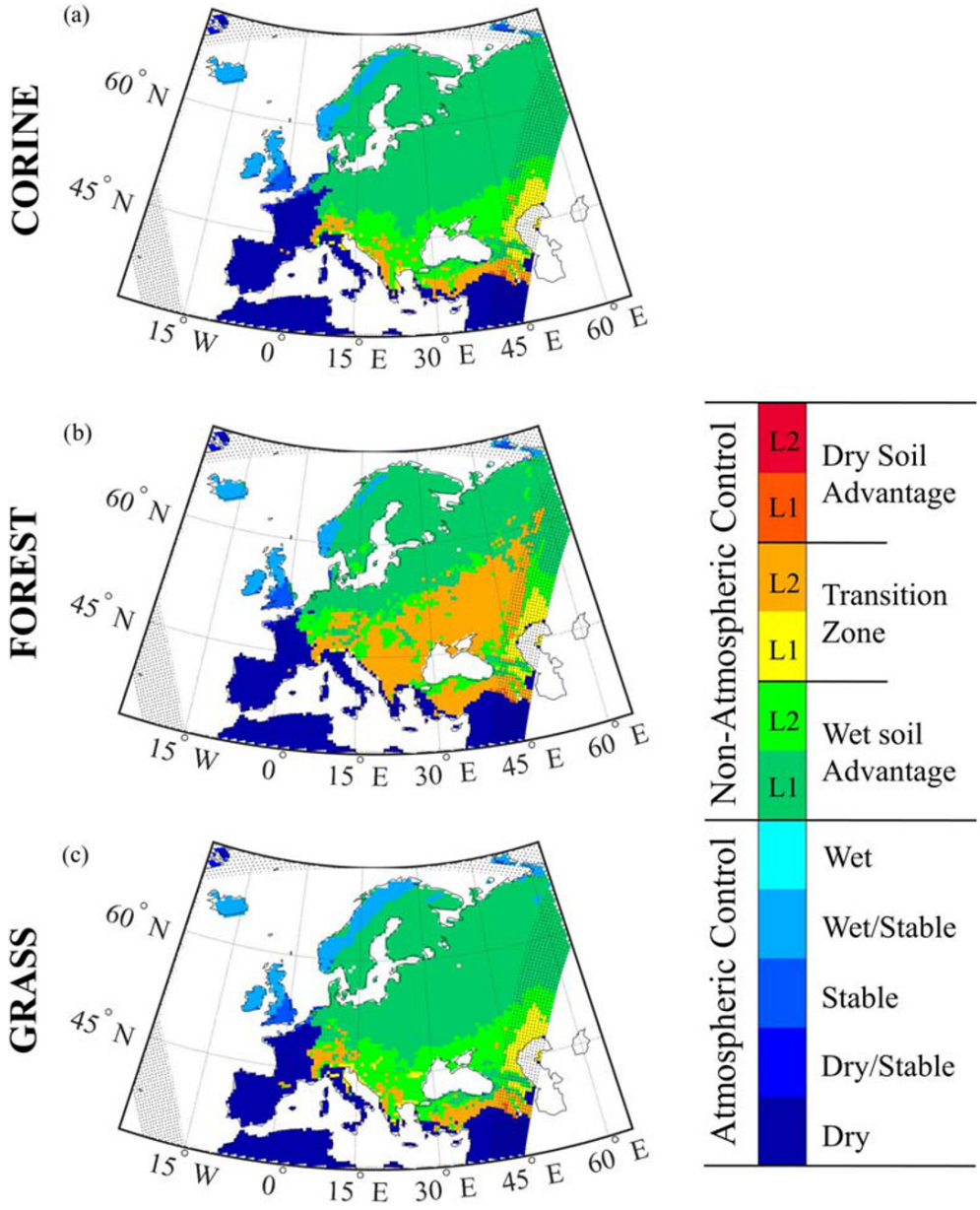


**Figure 3.** Long-term feedback regimes classified after the CTP-HIlow framework for (a) the CORINE run, (b) the FOREST scenario, and (c) the GRASS scenario. Atmospheric control is indicated in blue and the shadings depict the probable cause for atmospheric control. The nonatmospherically controlled feedback regime wet soil advantage is represented in green, the transition zone in yellow/orange, and the dry soil advantage in red. Levels 1 (L1) and 2 (L2) depict the strength of the signal. Level 1 cells have a strong signal, whereas the signal in level 2 cells is weaker.

In this RCM configuration, afforestation caused a decrease in EF (Figure 5b) everywhere except for western Europe and south of the Black Sea. An albedo decrease led to an increase in available energy, which was predominantly partitioned into sensible heat flux. The resulting significant destabilization and drying of the atmosphere at a significance level of 5% (Figures 4b and 4e) decreased the nAC days per summer. Thus, the feedback strength declined. The strongest impact of afforestation on the atmosphere appeared north of the Black Sea, where increases in CTP and $HI_{low}$ caused a significant loss of nAC days of up to 9.75%. The contrary effect was observed in western Europe, where EF increased by 0.03 and $HI_{low}$ decreased by −0.35°C. In consequence of these changes in western Europe, the fraction of nAC days increased significantly by up to 6.5% in some cells over the Alps.

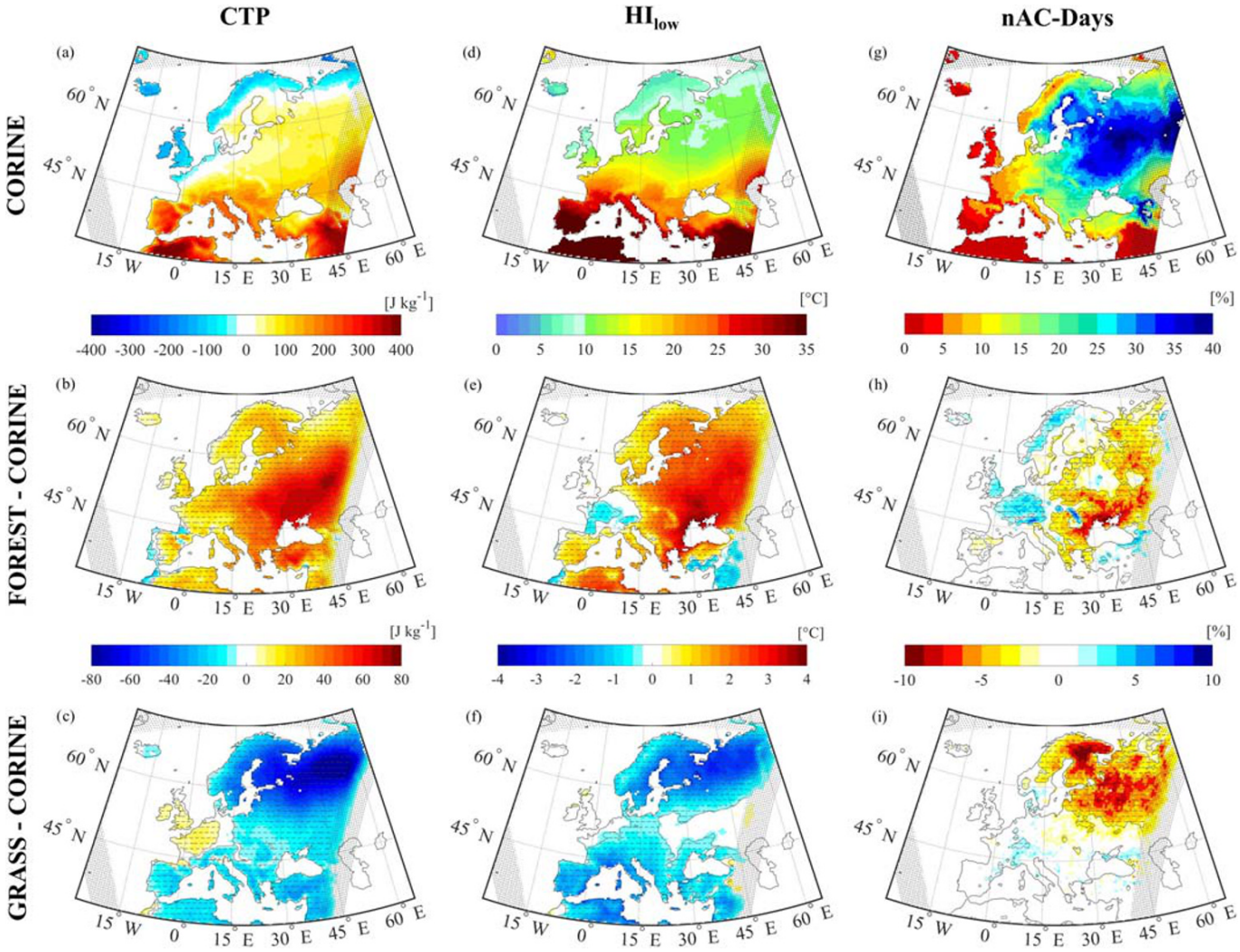


**Figure 4.** (a) Mean convective triggering potential (CTP) (J kg$^{-1}$) of the CORINE run, (b) the FOREST-CORINE difference in CTP, and (c) the GRASS-CORINE difference. (d) Mean summertime low-level humidity index (HI$_{low}$) (°C) of the CORINE run, (e) FOREST-CORINE difference in the HI$_{low}$, and (f) the GRASS-CORINE difference in HI$_{low}$. (g) The share of nonatmospherically controlled (nAC) days in summer (%), and (h and i) the corresponding differences between FOREST and CORINE and GRASS and CORINE, respectively. Dashed areas indicate statistical significance at the 5% level tested with a Student's *t* test.

In the FOREST run, the northern part of the feedback region was in wet soil advantage similarly to the baseline run. In the southeastern part of the feedback region, a transition occurred from wet soil advantage to transition zone level 2 (Figure 3b). Afforestation decreased the share of wet soil advantage days both relative to the nAC days in summer (Figure S1b) and relative to all summer days (Figure S2b) in most of the domain. The largest decrease appeared in eastern Europe. Simultaneously, afforestation increased the share of nAC days in transition zone and dry soil advantage (Figures S1e and S1h) leading to a weakening in the predominance of positive feedbacks and a change in the classification. Therefore, afforestation decreased not just the frequency of occurrence of nAC days (Figure 4h) in eastern Europe but also weakened the potential for positive feedbacks all over the domain. The combined effect is expected to result in a lower impact of the latent heat flux on local precipitation in comparison with the conditions of the baseline run.

The major impacts of deforestation on the summer L-A coupling strength occurred in the higher latitudes (Figures 4i, S2c, S2f, and S2i). The higher albedo of grassland generally initiated a decrease in net radiation (not shown) in Europe. In the high latitudes, the conversion of needleleaf forest to grassland caused a considerable increase in EF in GRASS (Figure 5c). This resulted from minor reductions in the latent heat

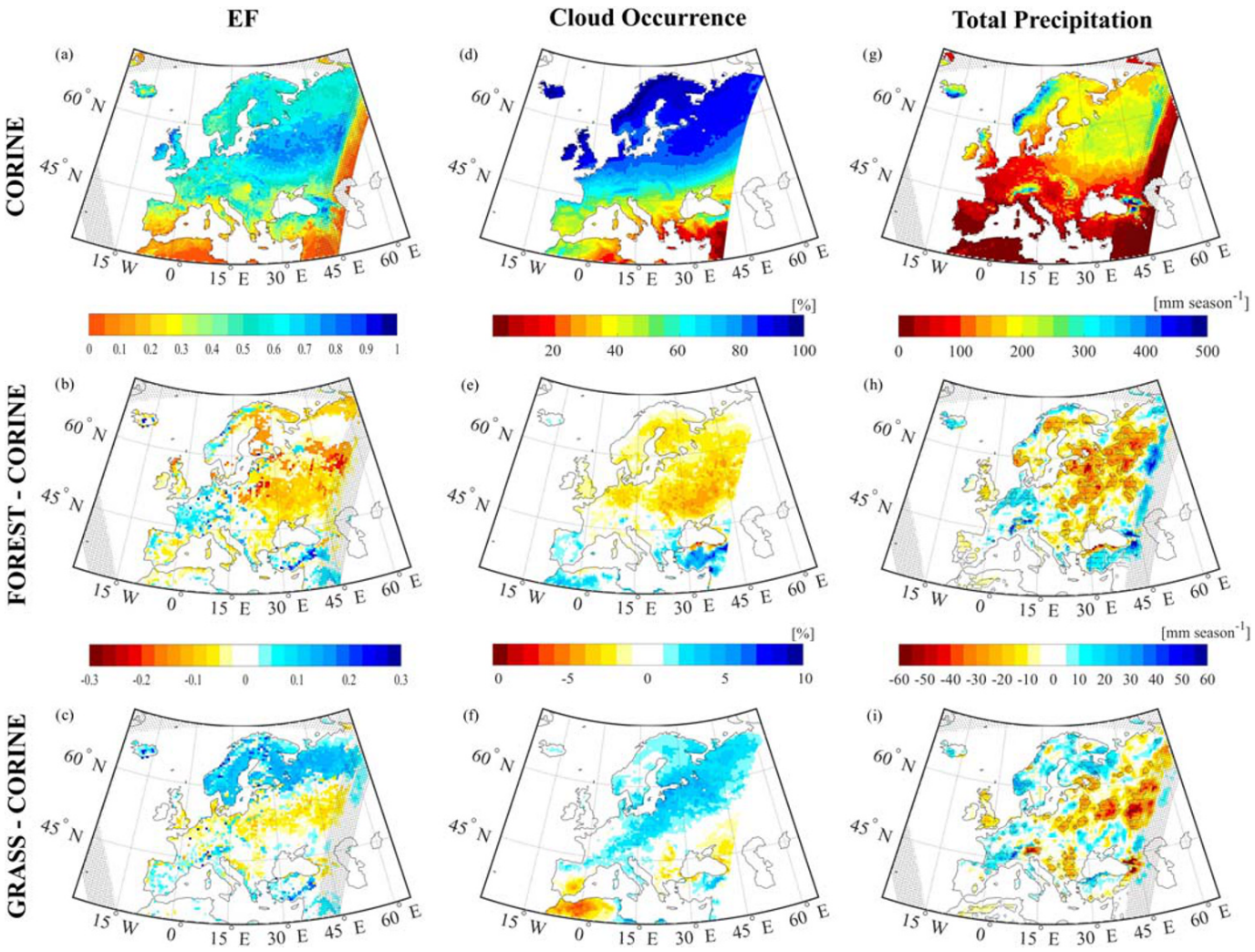


**Figure 5.** Results from CORINE and their differences due to afforestation (FOREST-CORINE) and deforestation (GRASS-CORINE) in summer. (a) Average evaporative fraction (EF), (b) difference in EF due to afforestation, (c) difference in EF due to deforestation, (d) frequency of occurrence of cloud coverage >3%, (e) difference in the occurrence of clouds due to afforestation, (f) difference in the occurrence of clouds due to deforestation, (g) mean seasonally accumulated, total precipitation, (h) difference of precipitation due to afforestation, and (i) difference of precipitation due to deforestation. All values correspond to the June–August average of the period 1986–2015.

flux and strong decreases in the sensible heat flux (not shown). The impacts of decreasing both the atmospheric instability and humidity deficit on the coupling were contradicting (Figure 4c and 4f). On the one hand, the cooling and moistening of the atmosphere indicates that relative humidity approaches saturation more frequently. Occasionally, up to 10% less summer days were in nAC compared to CORINE in the high-latitudes (Figure 4i), and wet AC days occurred more frequently. On the other hand, the predominance of the wet soil advantage was considerably strengthened in the nAC day partitioning (Figure S1c). Transition zone as well as dry soil advantage days occurred less frequently (Figures S1f and S1i). This means when a feedback was probable, wet surface conditions were very likely in favor for triggering precipitation rather than dry surface conditions. Consequently, the feedback region was mostly in levels 1 or 2 wet soil advantage in the GRASS run. In the rest of the domain, LULCC caused a net decrease in EF. This resulted from a reduction in the latent heat flux and minor reductions (cropland) or increases (mixed/deciduous forests) in the sensible heat flux. The changes in both the share of nAC days (average ± 0.3%) in summer (Figure 4i), and the share of summer days in wet or dry soil advantage or transition zone (Figures S2c, S2f, and S2i) were patchy and insignificant.

## 4. Effects on Clouds and Precipitation

Given the information about a potential coupling hot spot and a predominance of positive feedbacks, the question arises whether modifications in the surface flux partitioning from LULCC can be associated with changed cloud cover and total precipitation patterns in the predicted manner. Therefore, the aim of this chapter is to assess whether the sign of the response of cloud occurrence and precipitation distribution to afforestation and deforestation match the sign of EF differences.

### 4.1. Clouds

First, this chapter deals with modifications in the spatial distribution of cloud occurrence induced by LULCC. Second, differences in the frequency of occurrence of clouds in summer on different model heights are explored (Figure 5d). Coverage or occurrence of clouds was assumed, when the degree of coverage in an atmospheric layer exceeded 3% (threshold from Görsdorf & Seifert 2011).

In all experiments, clouds occurred most frequently in the high latitudes. The frequency (Figure 5d) and also the degree of coverage (not shown) decreased southward with the lowest frequencies south of the Black Sea. Besides the regional variance of cloud distribution, clouds also appeared in different altitudes depending on the region (Figure 6) in all experiments. In the high latitudes, lower-level clouds appeared with a higher frequency (Figures 6e and 6f) than in southern Europe (Figures 6i and 6j). Please note that by far most clouds appeared with a degree of coverage of 1 (meaning 100% of coverage) in most layers and in all subregions and experiments (Figures 6a and 6e; values of the CORINE run). In the highest model levels, cirrus clouds appeared with a maximum cloud coverage of 0.2.

Afforestation and deforestation had contrasting effects on clouds in Europe. While the atmospheric drying from afforestation (Figure 5e) coincided with fewer (Figure 5e) and less thick clouds (not shown), the atmospheric moistening from deforestation (Figure 5f) coincided with an increase in the frequency of cloud occurrence there (Figure 5f). The sign of the response to the respective LULCC scenario was consistent in the domain apart from southern Europe (Figures 5e and 5f). In the southern part of the domain, the response in cloud occurrence switched sign in both scenarios. Though the sign of differences was largely consistent, the magnitude of differences from both afforestation and deforestation varied, and the strongest effects from both LULCC scenarios appeared over the Eastern European Plain (Figures 5e and 5f).

Figure 6 shows the frequency distribution of cloud occurrence on model levels. The first row shows the frequency distribution of the whole domain, and the second row shows the results for the Eastern European Plain as an example for a relatively strong influence. The results for the Iberian Peninsula are shown as an example for a southern and rather dry region with weak potential surface influence. Similarly to the spatial averages, the changes in cloud coverage on different model levels were strongest over the Eastern European Plain relative to the rest of the domain (Figures 6g and 6h). Low-level clouds occurred less frequently in FOREST with a maximum loss of 6.5%. Midlevel clouds were slightly increased by 1.9%. Similarly, deforestation mostly impacted the occurrence of low-level clouds, which increased by +5% over the Eastern European Plain (Figure 6h). Both afforestation and deforestation barely influenced the occurrence of clouds over the Iberian Peninsula (Figures 5e and 5f). This is also reflected in the changes of cloud occurrence across different atmospheric heights (Figures 6k and 6l). In general, LULCC predominantly influenced the occurrence of low-level clouds in the whole domain.

### 4.2. Precipitation

This subsection examines the impacts of LULCC on total precipitation and precipitation probability. Further, it aims to estimate the connections of both EF and $HI_{low}$ changes with the magnitude of changes in precipitation and the probability for precipitation in dependence of the previously identified coupling regimes. The EF-precipitation and $HI_{low}$-precipitation connections were analyzed by applying an extended regression analysis (denoted as "Coupling Index" in Figures 7a and 7b) and looking at the coefficient of determination of the regression. These were introduced in section 2.4.2.

#### 4.2.1. Precipitation Distribution

All experiments showed a similar spatial distribution of total precipitation (Figure 5g; CORINE run exemplarily). Maxima in precipitation were mostly found in mountainous regions like the Alps, the Scandinavian Mountains, the Carpathians, and the Caucasus in all experiments.

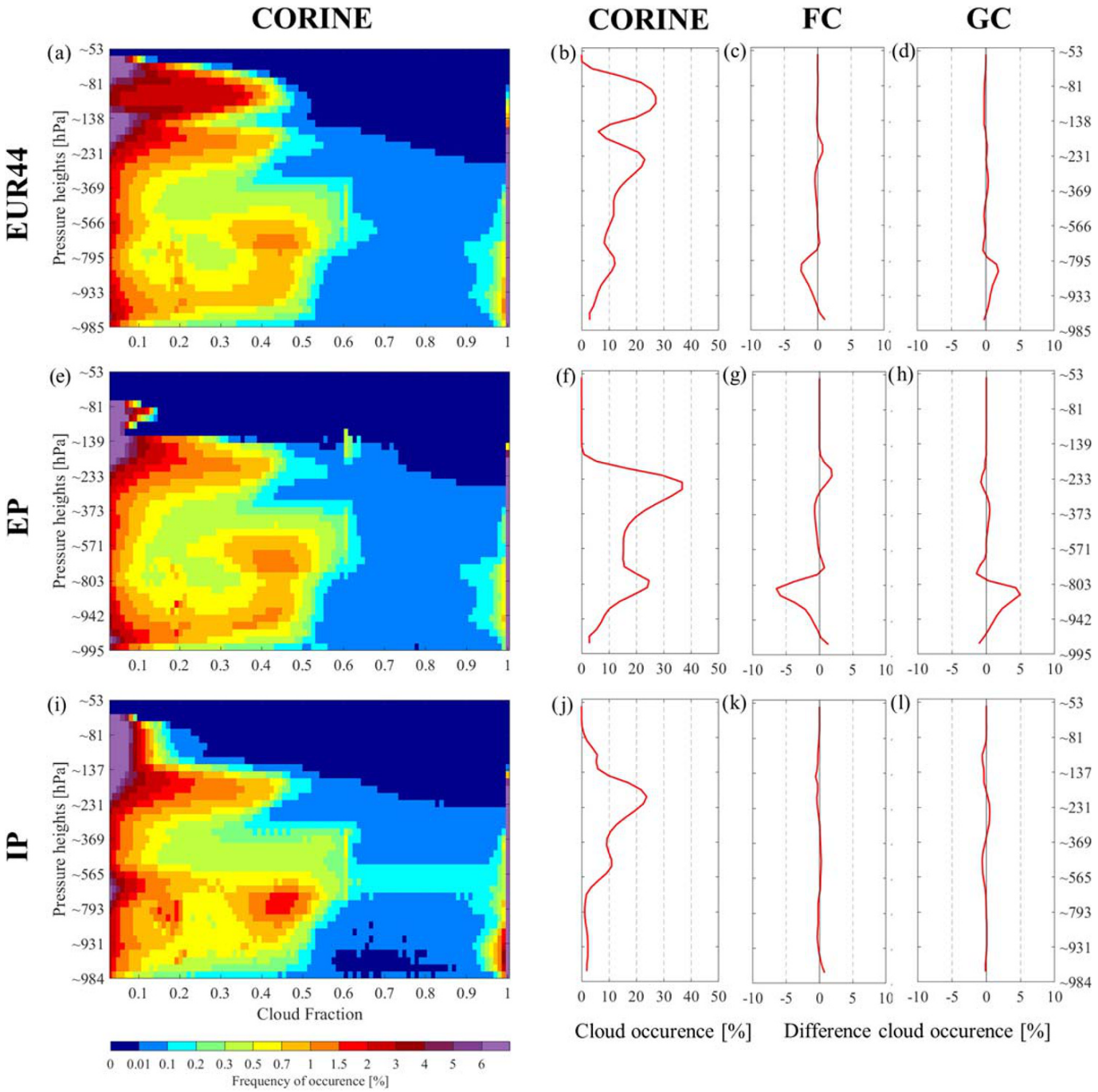


**Figure 6.** Cloud statistics (a) frequency distribution of different cloud fractions for each atmospheric layer (%) for the EURO-CORDEX domain (EUR44), taken into consideration are only cases with more than 3% cloud coverage, (b) the frequency of occurrence of clouds (degree of coverage >3%) regardless of the cloud fraction for EUR44, (c) the FOREST-CORINE (FC) difference in cloud occurrence on all model levels for EUR44, and (d) the respective difference for the difference GRASS-CORINE (GC) for EUR44. Similarly, (e–h) the results for the Eastern European Plain (EP) as an example for a rather wet region and (i–l) the results for the Iberian Peninsula (IP) as an example for a rather dry region.

Afforestation and deforestation initiated small but statistically significant differences in the total precipitation in summer. The impact on precipitation varied spatially in sign and magnitude (Figures 5h and 5i) in both scenarios. On the one hand, the LULCC impacted the day-to-day potential for local triggering of precipitation by modifying the flux partitioning (Figures 4h and 4i). On the other hand, an enhanced or

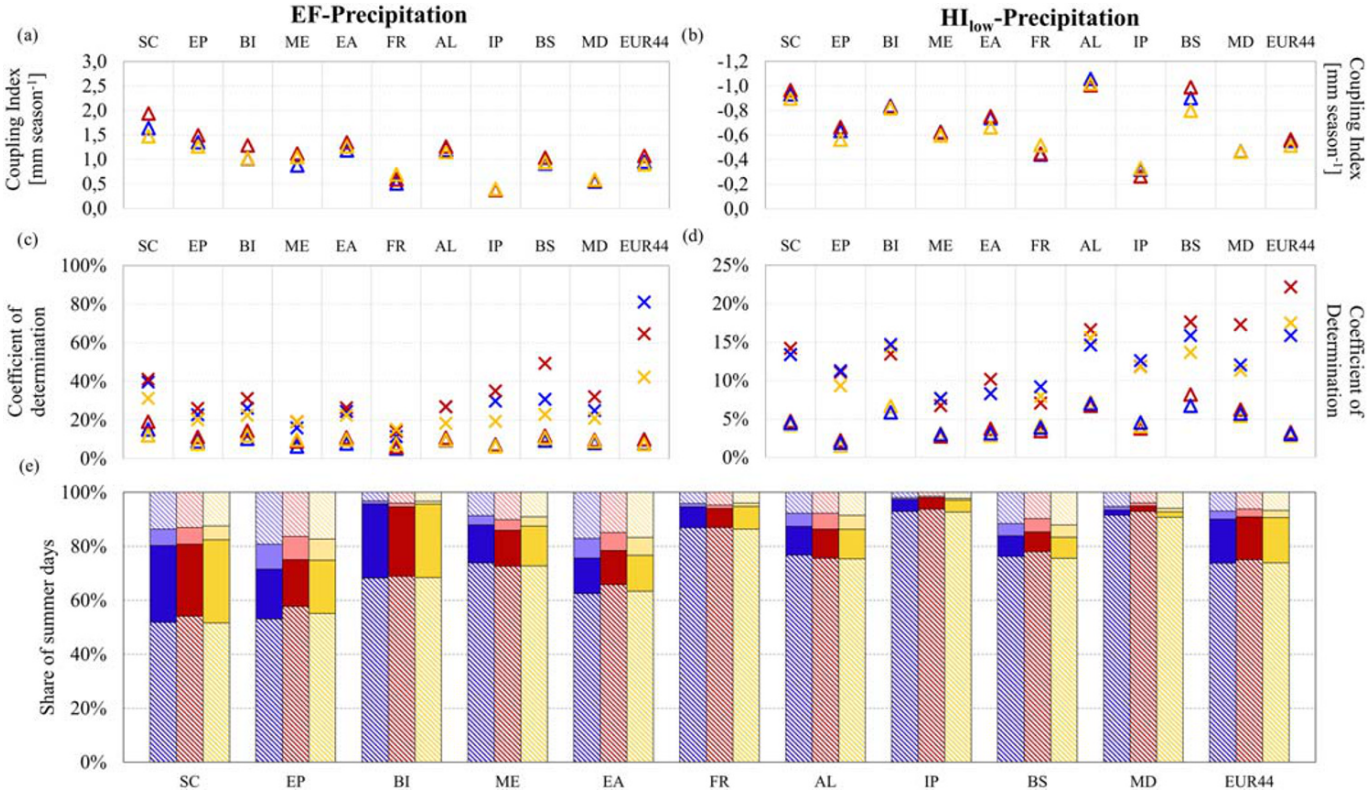


**Figure 7.** Subregion wise (a) coupling index between the evaporative fraction (EF) and daily total precipitation, (b) coupling index between the low-level humidity index ($HI_{low}$) and daily total precipitation, (c) coefficient of determination of regressions between EF and precipitation, and (d) coefficients of determination of regressions between $HI_{low}$ and precipitation. Triangles denote regional means and crosses denote regional maxima. (e) Fractions of summer days in atmospheric control (dark colors), with and without precipitation and nonatmospheric control (nAC; light colors). Fractions of AC and nAC days without precipitation are stripped. Colors are blue: CORINE, red: FOREST, and yellow: GRASS.

decreased transport of moisture and heat into the atmosphere modified the average atmospheric conditions (Figures 4b, 4c, 4e, and 4f). This modifies the probability for total precipitation and the preconditioning for convection triggering in the atmosphere. In eastern and northeastern Europe, both LULCC resulted in significant decreases in precipitation (significance level: 5%). With afforestation, lower EF and higher humidity deficits in the low-level atmosphere supported the reduction in precipitation (Figures 7a and 7b). The maximum decrease in precipitation occurred over the Eastern European Plain with −63.8 mm per season (Figure 5h). The local connections of precipitation with EF and $HI_{low}$ are further explored in section 4.2.2. In GRASS, the transition from cropland to grassland resulted in a lower EF (Figure 5c), which coincided with less precipitation in this region.

In western Europe, both LULCCs initiated a small increase in precipitation (Figures 5h and 5i). The increase in FOREST may be related with an increase in the latent heat flux, raising the moisture transport into the atmosphere. The additional moisture increased the relative humidity ($HI_{low}$) and considerably increased CAPE (not shown). Both quantities are expected to favor the occurrence of precipitation in the model, especially, as the Kain-Fritsch convection scheme is known to react sensitively to CAPE. The effect of deforestation was not as straightforward. The local connection between surface moisture and precipitation was particularly weak in France and impacts on atmospheric quantities like CAPE were small.

In the remaining regions, the impact of afforestation on precipitation diverged from the impact of deforestation. Afforestation caused an increase in rainfall over the Alps (+6.1 mm/season) and the Black Sea (+3.0 mm/season), while deforestation caused a decrease over the Alps (−2.1 mm/season) and the Black Sea (−2.6 mm/season). Both regions have a complex orography which possibly shapes the connection between surface moisture and precipitation (see section 4.2.2). In the high latitudes, the local connection

of the surface moisture appeared to be strong in all scenarios (Figures 7a and 7b). Thus, the surface drying from afforestation was expected to support a decrease in precipitation, whereas the moistening from deforestation rather supported an increase (Figures 5c and 5i).

#### 4.2.2. Surface Flux-Precipitation Connection

The strength of local connections of precipitation with EF and $HI_{low}$ was varying regionally. Please note that local refers to the connection between variables in a certain cell, here. Modifications in surface moisture and low-level humidity are likely to affect also the precipitation of neighboring cells, but these nonlocal influences are difficult to disentangle and they were not quantified within this study.

The coupling index of EF and precipitation was positive in all subregions and experiments (Figure 7a). This confirmed the conclusion drawn from the CTP-$HI_{low}$ framework, that surface moisture-precipitation feedbacks are generally more likely to be positive in the study area. A relatively strong connection between EF and precipitation emerged in the domain's Northeast as well as in regions with complex orography (Alps, Black Sea) in all experiments. In the rest of the domain, total precipitation was less correlated with EF (Figure 7a). The weakest coupling indices were found over southern Europe and France in each experiment (Figure 7a), which was characterized by rather dry conditions. Since the coupling index was low, differences in the precipitation of the different scenarios (Figures 5h and 5i) were not locally attributable to changes in the surface flux partitioning there. However, the modifications in the surface flux partitioning impacted the humidity deficit (Figures 4e and 4f), and hence, they changed the preconditioning for convection triggering and for precipitation development in general (Figure 7b) during the 30-year period.

Though the Black Sea region also faced comparably dry conditions (Figure 4d), the coupling index was considerably higher than in the rest of southern Europe. The presence of mountains was expected to support the vertical motion of air through orographic lifting. Since orography supported the lifting of moist air, more moist surface and low-level atmospheric conditions presumably foster the probability for local precipitation. This is reflected in the EF-precipitation and the $HI_{low}$-precipitation connections (Figure 7). Both the coupling indices and the coefficients of determination were high in relation to the rest of the domain. All of the maximum values (crosses in Figures 7c and 7d) were observed over mountains. This effect was also observable over the Alps and the Scandinavian mountains.

The share of variance in precipitation explainable by EF amounted to 7.8%, averaged over the domain (FOREST: 10.0% and GRASS: 7.5%) with strong variance between subregions (Figure 7c). While the lowest share of explained variance was found in Central Europe, the largest share was apparent in the high latitudes in all scenarios. In individual cells, up to 40% of the variance in precipitation is explainable by EF over needleleaf forest, there (Figure 7c). However, the pattern of the coefficient of determination did not follow the distribution of the share of nAC days (Figure 4g). Rather, it reflected features of the respective vegetation map. Especially over needleleaf forest, the fraction of explained variance was high, whereas over cropland it was clearly lower (data not shown). Afforestation generally tended to enhance the share of variance in precipitation explainable by the EF—everywhere except for the Alps. Deforestation initiated a mixed response in the EF-precipitation relationship (Figure 7c). On the one hand, in the high latitudes and over the Iberian Peninsula, the share of variance in precipitation explainable by EF decreased due to the conversion from needleleaf forest to grassland. On the other hand, in central and southeastern Europe, converting forests and croplands to grassland increased the variance explained by EF. These findings confirm the conclusion that LULCC has an impact on coupling strength itself. It also highlights the importance of considering the concrete type of vegetation transition.

#### 4.2.3. Atmospherically Versus Nonatmospherically Controlled Days

This subsection describes the difference in precipitation probability between AC and nAC days for the subregions. Table 2 depicts the probability for precipitation on AC and nAC days, as well as the proportion of the total precipitation that fell on nAC days. Please note that precipitation on nAC days is not equated with convective precipitation which was triggered by the land surface.

Although the majority of summer days were AC in every grid cell and most precipitation fell on AC days in absolute terms in each subregion (Figure 7e), the probability for precipitation was clearly higher on nAC days than on AC days. This applied for every subregion except for Scandinavia and the British Isles in all experiments (Table 2). In southern Europe, where precipitation occurrence was rare, the probability for precipitation was considerably higher on nAC days than on AC days (Table 2). In the Mediterranean, the share

Journal of Geophysical Research: Atmospheres

10.1029/2019JD031989

**Table 2**

*Average Evaporative Fraction (EF) and Probability for Precipitation for Atmospherically Controlled (AC) and Nonatmospherically Controlled (nAC) Days in Each PRUDENCE-Region and the Percentage of Total Precipitation Actually Falling on nAC Days for Each Scenario*

| | CORINE | | | | | FOREST | | | | | GRASS | | | | |
|---|---|---|---|---|---|---|---|---|---|---|---|---|---|---|---|
| | AC | | nAC | | Share of $P$ on nAC days | AC | | nAC | | Share of P on nAC days | AC | | nAC | | Share of $P$ on nAC days |
| | EF | Probability for $P^a$ | EF | Probability for $P^a$ | | EF | Probability for $P^a$ | EF | Probability for $P^a$ | | EF | Probability for $P^a$ | EF | Probability for $P^a$ | |
| SC | 0.58 | 0.46 (0.26; 0.77) | 0.57 | 0.41 (0.22; 0.67) | 19.7% | 0.55 | 0.42 (0.19; 0.84) | 0.53 | 0.41 (0.13; 0.80) | 21.6% | 0.65 | 0.47 (0.41; 0.74) | 0.64 | 0.39 (0.27; 0.63) | 14.9% |
| EP | 0.60 | 0.34 (0.06; 0.59) | 0.65 | 0.40 (0.09; 0.55) | 34.9% | 0.54 | 0.30 (0.06; 0.66) | 0.60 | 0.41 (0.10; 0.69) | 34.7% | 0.65 | 0.34 (0.07; 0.59) | 0.67 | 0.39 (0.08; 0.55) | 30.2% |
| BI | 0.67 | 0.36 (0.14; 0.65) | 0.62 | 0.35 (0.11; 0.63) | 4.9% | 0.63 | 0.34 (0.24; 0.74) | 0.59 | 0.35 (0.08; 0.77) | 6.4% | 0.65 | 0.36 (0.14; 0.69) | 0.60 | 0.33 (0.05; 0.68) | 4.6% |
| ME | 0.55 | 0.17 (0.05; 0.37) | 0.58 | 0.29 (0.12; 0.48) | 23.3% | 0.58 | 0.17 (0.03; 0.49) | 0.60 | 0.33 (0.09; 0.67) | 25.8% | 0.54 | 0.18 (0.05; 0.53) | 0.57 | 0.31 (0.07; 0.64) | 22.6% |
| EA | 0.53 | 0.19 (0.04; 0.44) | 0.60 | 0.33 (0.10; 0.51) | 36.3% | 0.48 | 0.19 (0.03; 0.57) | 0.57 | 0.35 (0.09; 0.68) | 34.9% | 0.51 | 0.20 (0.03; 0.54) | 0.56 | 0.32 (0.07; 0.60) | 33.6% |
| FR | 0.47 | 0.10 (0.03; 0.33) | 0.52 | 0.30 (0.09; 0.62) | 21.8% | 0.51 | 0.09 (0.02; 0.39) | 0.56 | 0.26 (0.11; 0.60) | 24.3% | 0.46 | 0.10 (0.03; 0.48) | 0.51 | 0.30 (0.05; 0.72) | 20.8% |
| AL | 0.47 | 0.15 (0.03; 0.48) | 0.55 | 0.47 (0.11; 0.80) | 33.1% | 0.49 | 0.16 (0.02; 0.55) | 0.60 | 0.51 (0.13; 0.83) | 37.0% | 0.50 | 0.16 (0.02; 0.56) | 0.60 | 0.45 (0.06; 0.77) | 33.7% |
| IP | 0.27 | 0.05 (0.01; 0.43) | 0.43 | 0.34 (0.07; 0.81) | 19.5% | 0.25 | 0.05 (0.01; 0.52) | 0.38 | 0.34 (0.05; 0.91) | 17.8% | 0.28 | 0.05 (0.01; 0.49) | 0.43 | 0.31 (0.09; 0.78) | 20.2% |
| BS | 0.33 | 0.10 (0.02; 0.58) | 0.47 | 0.35 (0.12; 0.74) | 34.7% | 0.35 | 0.09 (0.01; 0.67) | 0.50 | 0.42 (0.10; 0.87) | 36.2% | 0.36 | 0.10 (0.01; 0.67) | 0.47 | 0.34 (0.07; 0.82) | 33.4% |
| MD | 0.27 | 0.06 (0.01; 0.51) | 0.46 | 0.35 (0.10; 0.77) | 41.4% | 0.25 | 0.06 (0.01; 0.61) | 0.46 | 0.39 (0.11; 0.82) | 38.4% | 0.28 | 0.05 (0.01; 0.62) | 0.43 | 0.32 (0.06; 0.82) | 40.8% |
| EUR44 | 0.29 | 0.17 (0.01; 0.58) | 0.59 | 0.38 (0.10; 0.57) | 28.1% | 0.28 | 0.16 (0.01; 0.67) | 0.56 | 0.40 (0.09; 0.71) | 28.6% | 0.31 | 0.18 (0.01; 0.62) | 0.60 | 0.36 (0.07; 0.59) | 24.0% |

*Note*. SC = Scandinavia, EP = Eastern European Plain, BI = British Isles, ME = Mid-Europe, EA = Eastern Europe, FR = France, AL = Alps, IP = Iberian Peninsula. BS = Black Sea, MD = Mediterranean, and EUR44 = EURO-CORDEX domain.

[a]The probability for precipitation (fraction ranging from 0 to 1) is given for all days, and the values in brackets denote the probability on days only with low (0–0.25) and high (0.75–1) values of EF.

of total summer precipitation falling on nAC days corresponded to about 40% in all experiments, even though the occurrence of nAC days was rare in summer. However, the total amount of precipitation was low and so was the net effect of the surface on precipitation. In central and eastern Europe, nAC days had a higher probability for precipitation than AC days, as well, but the differences between AC and nAC days were smaller than in the dry-regions. Between 20% and 33% of the total precipitation per season fell on nAC days (Table 2).

In Scandinavia and over the British Isles, the probability for precipitation was generally high and did not differ considerably between AC and nAC days. Over these two regions, the majority of AC days were wet and stable, and more than 80% or 95%, respectively, of their total precipitation amounts occurred on AC days in all experiments (Figure 7e). A very high relative humidity (low $HI_{low}$) fostered precipitation on the wet AC days and explained why the probability is similar on AC and the wet soil advantage dominated nAC days. Presumably, the surface flux partitioning was not decisive for the triggering of precipitation on these days. However, investigating the probability for precipitation for different EF bins showed a divergence in the probability of precipitation for different ranges of EF on both AC and nAC days (not shown). The same applied for the daily amount of precipitation. Both increased gradually from very low (probability: 0.01–0.26) to very high EF values (probability: 0.37–0.75) throughout the domain. This did not apply for Scandinavia and the British Isles. In these regions, the probability for precipitation and the amount of rainfall were both higher with a clearly dominating sensible heat flux ($EF < 0.25$) than with a slightly dominating to equal share of sensible heat ($0.25 < EF < 0.5$). This indicated that the surface flux partitioning could still support or inhibit precipitation from large-scale systems, even though they are not decisive for its occurrence.

## 5. Discussion

Strong, positive, local surface moisture-precipitation feedbacks were identified under continental climate in northeastern Europe by using the CTP-$HI_{low}$ framework in all experiments (section 3.1). Under oceanic, Mediterranean or arctic climate, large-scale atmospheric forcings predominantly inhibit local feedbacks—in accordance with the argumentation of Findell and Eltahir (2003b). The region of potentially strong coupling roughly coincided with the hot spot region of soil moisture-precipitation coupling that Koster et al. (2004) found in their global L-A coupling strength ensemble study in Europe. The robustness of the feedback region's location and the predominant sign of potential feedbacks were further examined with a sensitivity test (description in supporting information). In the summer of 1986, the initial temperature and moisture profiles of the baseline run were perturbed before calculating CTP and $HI_{low}$ and performing the classification. The degrees of temperature and moisture perturbation were chosen to mimic a realistic model spread in moisture and temperature variance for the current climate in Europe. Extremer modifications were tested, as well. Perturbations within the realistic range slightly shifted the coupling hot spot, though it was not moved to a different European region (Figures S3 and S5). Therefore, the location of the coupling hot spot and also the predominance of positive feedbacks are considered robust under current climatic conditions.

The L-A coupling strength is generally a rather model specific quantity (Pitman et al., 2009), whose results may be influenced by the choice of PBL and convection parameterization (Hirsch et al., 2015; Milovac et al., 2016). In section 3.2, it was shown that both LULCC scenarios modified the potential feedback strength by changing the relative humidity and the instability in the early-morning boundary layer. In the presented model configuration, the frequency of potential nAC days decreased in both scenarios. Thus, the probability for a surface influence on precipitation is estimated to decrease from both afforestation and deforestation. Furthermore, the LULCC changed nAC day partitioning between the feedback categories (Figures S1 and S2). Afforestation decreased EF as a result of a dominant albedo effect, and a disproportionately strong increase in the sensible heat flux in most European regions. This finally led to a weakened wet soil advantage in the domain (Figure S1). In GRASS, most transitions to grassland caused a net decrease in the EF. The only exception was the transition from evergreen needleleaf forest to grassland, which mostly occurs in the high latitudes. It caused a loss in available energy as well as an increase in EF which originated from a stronger decrease in the sensible heat flux than in the latent heat flux. The transition from needleleaf forest to grassland also caused the largest impact on the coupling strength due to deforestation in the high

latitudes. On the one hand, feedback days occurred less frequently in summer. On the other hand, it strengthened the predominance of the wet soil advantage on nAC days (Figure S1c). The LULCC responses in surface flux partitioning mostly coincided with the findings of Duveiller, Forzieri, et al. (2018) who examined the effects of a suite of vegetation transitions on the radiation and energy balances at the land surface.

Nevertheless, Davin et al. (2020) demonstrated a divergence in the temperature response to afforestation between the models of the LUCAS ensemble, in which these simulations were included (their WRFb-NoahMP). They showed that the temperature response is directly linked to how afforestation modified the surface flux partitioning in the models. They attributed this inconsistency to a lack of agreement in the calculation of evapotranspiration between models (de Noblet-Ducoudré et al., 2012; Lejeune et al., 2017). Simulations with, for example, the RCA model rather simulated an increase in EF and a concurrent decrease in temperature in response to afforestation in Europe, caused by a net evaporative cooling effect (e.g., Belušić et al., 2019; Davin et al., 2020; Strandberg & Kjellström, 2019). The disagreement in the temperature response to afforestation has implications for the conclusions drawn on the LULCC effects on the coupling strength. The sensitivity test showed that the average temperature and moisture conditions impacted the coupling strength (Figures S5 and S6) and the occurrence of the feedback categories (Figures S3 and S4). While warming and drying enhanced the number of days in dry AC and transition zone (Figure S3i), cooling and moistening enhanced the wet and stable AC (Figure S3a). Hence, the temperature response of a model to LULCC (and likely also the moisture response) is expected to determine how these LULCC modify the coupling. Therefore, the conclusions drawn on the afforestation and deforestation effects on the coupling strength are specific for this model configuration. Further analysis would benefit from the use of an ensemble.

Both LULCC scenarios yielded differences in cloud occurrence and precipitation. The predominating decrease in EF from afforestation was accompanied by a significant decrease in relative humidity in the lower PBL and a concurrent reduction in low-level cloud occurrence and cloud coverage in northeastern and central Europe (section 4.1). Concomitantly, the total precipitation was significantly lower in confined areas within the hot spot region and over mountains (section 4.2.1). In western Europe, afforestation considerably increased relative humidity and CAPE what could be an explanation for the additional precipitation in this region. Although the low-level relative humidity and the occurrence of low-level clouds were significantly increased in the Northeast in GRASS, the total precipitation was lower compared to the baseline run in that area. One possible explanation could be that less CAPE is available for convection triggering over grassland. The higher albedo of grassland reduces the amount of available energy for flux partitioning, wherefore less precipitation is triggered.

Over the study period, the surface fluxes could influence the probability and amount of total precipitation in three different ways. First, moisture and energy enter into the atmosphere throughout the day and either trigger deep convection by increasing the atmospheric humidity through the input of latent heat (e.g., Dirmeyer, 2011) or support PBL growth by adding sensible heat (Dirmeyer et al., 2014; Taylor et al., 2012) (section 4.2.1). Second, the surface fluxes impact the humidity and stability in the residual layer in the seasonal average of June–August in 1986–2015 (section 4.2.1). Hence, the preconditioning changes to more or less favorable conditions for convection and for precipitation in general. Nonlocal effects of the background climate are likely (Winckler et al., 2017), but further research is necessary to identify and quantify remote effects. Third, the surface fluxes may enhance or suppress precipitation from large-scale circulations on days with very humid atmospheric conditions, which mainly occur in Scandinavia and over the British Isles (section 4.2.3). Precipitation is known to dominantly occur there due to either large-scale circulations or cyclones (Belušić et al., 2019; Pfahl & Wernli, 2012) rather than due to local triggering of convection. However, the prevailing EF on a certain day still influences the occurrence and to a minor extent the intensity of precipitation in summer (not shown). It is notable that very low ($EF < 0.25$) values of EF were observed to favor the occurrence of precipitation and rather than intermediate ($0.25 < EF < 0.5$) ones in the wet regions.

Altogether, an increase in the EF coincides with an increase in precipitation, pointing toward reinforcing interactions between surface fluxes and precipitation in the whole study area. The strongest changes in precipitation were predominantly located over mountains and within the strong coupling area which was previously identified with the CTP-$HI_{low}$ framework. Nevertheless, the change in EF distribution from both

LULCC scenarios was small and significant impacts on precipitation occurred only in confined areas. This finding coincides with previous LULCC studies targeting precipitation in Europe, who also found that extreme afforestation had only minor impacts on precipitation (e.g., Seneviratne et al., 2013).

## 6. Summary

In this study, we investigated the potential L-A coupling strength in connection with actually modeled feedbacks between the turbulent surface fluxes and both clouds and precipitation patterns for the European summer. The study aimed at identifying land surface-precipitation coupling hot spots in dependence on land cover. Further, the intention was to test whether the strongest impacts of LULCC on clouds and precipitation were observed in regions where strong coupling is to be expected. The results give a range of hypothetical maximum impacts of LULCC by comparing the outcome of an extreme afforestation and deforestation scenario with a realistic baseline. To the knowledge of the authors, this is the first study for Europe that addresses L-A coupling strength in terms of surface flux-precipitation feedbacks on the regional scale and in dependence of land cover.

A coupling hot spot was identified in the northeast of the simulation domain mostly covering the Eastern European Plain and parts of Scandinavia and Eastern Europe. Feedbacks were predicted to be predominantly positive in all experiments. The scenarios mainly diverge in the fraction of potential feedback days and, hence, the likelihood of convection initiation by the land surface. With this model configuration, complete afforestation reduced the likelihood of land surface contribution to the triggering of convection in the east of the domain and slightly enhanced it in the west. Conversely, deforestation caused a significant reduction in the likelihood for a land surface impact in the high latitudes. Modeled impacts of the LULCC on clouds and total precipitation confirmed a predominance of reinforcing interactions, and a decrease in EF tended to be accompanied by a decrease in low-level clouds and total precipitation in all European subregions. This is on one hand attributable to local impacts of the surface fluxes during the day and, on the other hand, also to modifications of the boundary layer conditions in the 30 year average.

The presented analyses serve as a test bed for future studies on the impacts of realistic LULCC on the climate, keeping the focus on the impacts of L-A feedbacks and their modifications to climate change. Since studies based on a single RCM have limited generalizability, a possible extension of this work is a multimodel ensemble analysis of the L-A coupling strength to improve the robustness of the obtained results. Besides impacts of PBL and convection parameterization (Chen et al., 2017; Hirsch et al., 2015; Milovac et al., 2016) on estimating the L-A coupling strength, further dependencies, for example, on increasing the model resolution, and, hence, also the resolution of the land surface, to convection-permitting scale, or dynamic vegetation development (Ingwersen et al., 2018), are conceivable. Davin et al. (2020) highlight the need to understand the discrepancies in modeling the evapotranspiration. This is a prerequisite to understanding how and why feedbacks are spatially and temporally variable and how clouds and precipitation are impacted by LULCC. Additional variables, which characterize the boundary layer structure, need to be included in the analysis in order to improve the understanding of different links between the land surface and precipitation. Further studies targeting the understanding of biogeophysical impacts of land cover changes on the climate will be conducted in the scope of LUCAS. The sensitivity of the feedback strength and the sign of feedbacks to differences in atmospheric temperature and moisture will be further explored in a comprehensive sensitivity study. These findings as well as findings from further studies within LUCAS have provided a springboard for future L-A feedback analyses in Europe and improved our understanding about implications of LULCC on the climate.

## Appendix A: Definitions of CTP and $HI_{low}$

*Convective Triggering Potential*. The CTP (J $kg^{-1}$) is a measure of the atmospheric instability. It represents the deviation of the modeled temperature profile ($T_{env}$) from the moist adiabatic lapse rate between 100 and 300 hPa above ground (formula from Ferguson & Wood 2011).

$$CTP = \int_{z_{p_{sfc}-100}}^{z_{p_{sfc}-300}} g\left(\frac{T_{parcel} - T_{env}}{T_{env}}\right) dz,$$

with $z_{psfc-300}$ and $z_{psfc-100}$ representing the height at surface pressure $p_{sfc}$ − 300 hPa and $p_{sfc}$ − 100 hPa,

respectively. $T_{parcel}$ represents the temperature of an air parcel, which is lifted along the moist adiabatic lapse rate originating from 100 hPa above the surface and $g$ is the gravitational acceleration.

*Low-Level Humidity Index*. The $HI_{low}$ (°C) measures the humidity deficit in low-level air. It corresponds to the sum of dew point depressions at 50 and 150 hPa above ground.

$$HI_{low} = \left(T_{sfc-50} - T_{d,sfc-50}\right) + \left(T_{sfc-150} - T_{d,sfc-150}\right)$$

*Data*. CTP and $HI_{low}$ are calculated from daily early morning atmospheric profiles of temperature and humidity. Early morning profiles represent the state of the atmosphere within the hour of sunrise. Here this is defined as the time step of each day, where incoming shortwave radiation is first larger than zero. It is used as index to extract the temperature and humidity profiles of the local hour of sunrise from hourly model output for each cell and each day.

## Data Availability Statement

The alternative land cover maps and the NCL scripts used for the computation of the CTP-$HI_{low}$ framework as well as the name lists can be downloaded from the repository link (http://doi.org/10.5281/zenodo.3722520).

**Acknowledgments**
The research of this study was funded by the Anton and Petra Ehrmann-Stiftung Research Training Group "Water-People-Agriculture". We thank the three anonymous reviewers for their comments and helpful remarks on the manuscript. We thank Thomas Schwitalla and Oliver Branch for their many fruitful discussions and helpful suggestions. Furthermore, we acknowledge support by the state of Baden-Württemberg through bwHPC. We acknowledge ECMWF for providing ERA-Interim data on model levels.

## References

Bagley, J. E., Desai, A. R., Harding, K. J., Snyder, P. K., & Foley, J. A. (2014). Drought and deforestation: Has land cover change influenced recent precipitation extremes in the Amazon? *Journal of Climate*, *27*(1), 345–361. https://doi.org/10.1175/JCLI-D-12-00369.1

Baldocchi, D., Kelliher, F. M., Black, T. A., & Jarvis, P. (2000). Climate and vegetation controls on boreal zone energy exchange. *Global Change Biology*, *6*(S1), 69–83. https://doi.org/10.1046/j.1365-2486.2000.06014.x

Bauer, H.-S., Schwitalla, T., Wulfmeyer, V., Bakhshaii, A., Ehret, U., Neuper, M., & Caumont, O. (2015). Quantitative precipitation estimation based on high-resolution numerical weather prediction and data assimilation with WRF—A performance test. *Tellus A: Dynamic Meteorology and Oceanography*, *67*(1), 25047. https://doi.org/10.3402/tellusa.v67.25047

Belušić, D., Fuentes-Franco, R., Strandberg, G., & Jukimenko, A. (2019). Afforestation reduces cyclone intensity and precipitation extremes over Europe. *Environmental Research Letters*, *14*(7), 074009. https://doi.org/10.1088/1748-9326/ab23b2

Boisier, J. P., de Noblet-Ducoudré, N., Pitman, A. J., Cruz, F. T., Delire, C., van den Hurk, B. J. J. M., et al. (2012). Attributing the impacts of land-cover changes in temperate regions on surface temperature and heat fluxes to specific causes: Results from the first LUCID set of simulations: BIOGEOPHYSICAL IMPACTS OF LULCC. *Journal of Geophysical Research*, *117*, D12116. https://doi.org/10.1029/2011JD017106

Bonan, G. (2016). *Ecological Climatology: Concepts and Applications* (3rd ed.). Cambridge: Cambridge University Press. https://doi.org/10.1017/CBO9781107339200

Bonan, G. B. (2008). Forests and climate change: Forcings, feedbacks, and the climate benefits of forests. *Science*, *320*(5882), 1444–1449. https://doi.org/10.1126/science.1155121

Chen, L., & Dirmeyer, P. A. (2017). Impacts of land-use/land-cover change on afternoon precipitation over North America. *Journal of Climate*, *30*(6), 2121–2140. https://doi.org/10.1175/JCLI-D-16-0589.1

Chen, L., Dirmeyer, P. A., Tawfik, A., & Lawrence, D. M. (2017). Sensitivities of land cover–precipitation feedback to convective triggering. *Journal of Hydrometeorology*, *18*(8), 2265–2283. https://doi.org/10.1175/JHM-D-17-0011.1

Cherubini, F., Huang, B., Hu, X., Tölle, M. H., & Strømman, A. H. (2018). Quantifying the climate response to extreme land cover changes in Europe with a regional model. *Environmental Research Letters*, *13*(7), 074002. https://doi.org/10.1088/1748-9326/aac794

Christensen, J. H., & Christensen, O. B. (2007). *A Summary of the PRUDENCE Model Projections of Changes in European Climate by the End of This Century*. Copenhagen, Denmark: Danish Meteorological Institute.

Davin, E. L., & de Noblet-Ducoudré, N. (2010). Climatic impact of global-scale deforestation: Radiative versus nonradiative processes. *Journal of Climate*, *23*(1), 97–112. https://doi.org/10.1175/2009JCLI3102.1

Davin, E. L., Rechid, D., Breil, M., Cardoso, R. M., Coppola, E., Hoffmann, P., et al. (2020). Biogeophysical impacts of forestation in Europe: First results from the LUCAS (land use and climate across scales) regional climate model intercomparison. *Earth System Dynamics*, *11*(1), 183–200. https://doi.org/10.5194/esd-11-183-2020

Davin, E. L., Seneviratne, S. I., Ciais, P., Olioso, A., & Wang, T. (2014). Preferential cooling of hot extremes from cropland albedo management. *Proceedings of the National Academy of Sciences*, *111*(27), 9757–9761. https://doi.org/10.1073/pnas.1317323111

de Noblet-Ducoudré, N., Boisier, J.-P., Pitman, A., Bonan, G. B., Brovkin, V., Cruz, F., et al. (2012). Determining robust impacts of land-use-induced land cover changes on surface climate over North America and Eurasia: Results from the first set of LUCID experiments. *Journal of Climate*, *25*(9), 3261–3281. https://doi.org/10.1175/JCLI-D-11-00338.1

Dee, D. P., Uppala, S. M., Simmons, A. J., Berrisford, P., Poli, P., Kobayashi, S., et al. (2011). The ERA-Interim reanalysis: Configuration and performance of the data assimilation system. *Quarterly Journal of the Royal Meteorological Society*, *137*(656), 553–597. https://doi.org/10.1002/qj.828

Dione, C., Lothon, M., Badiane, D., Campistron, B., Couvreux, F., Guichard, F., & Sall, S. M. (2014). Phenomenology of Sahelian convection observed in Niamey during the early monsoon: Sahelian convection during the early monsoon. *Quarterly Journal of the Royal Meteorological Society*, *140*(679), 500–516. https://doi.org/10.1002/qj.2149

Dirmeyer, P. A. (2011). The terrestrial segment of soil moisture-climate coupling: Soil moisture-climate coupling. *Geophysical Research Letters*, *38*, L16702. https://doi.org/10.1029/2011GL048268

Dirmeyer, P. A., Jin, Y., Singh, B., & Yan, X. (2013). Evolving land–atmosphere interactions over North America from CMIP5 simulations. *Journal of Climate*, *26*(19), 7313–7327. https://doi.org/10.1175/JCLI-D-12-00454.1

Dirmeyer, P. A., Wang, Z., Mbuh, M. J., & Norton, H. E. (2014). Intensified land surface control on boundary layer growth in a changing climate: Dirmeyer et al.: Land-PBL feedback in a changing climate. *Geophysical Research Letters*, *41*, 1290–1294. https://doi.org/10.1002/2013GL058826

Dittmann, E., & Deutscher Wetterdienst (Eds.) (1995). *Objektive Wetterlagenklassifikation*. Dt. Wetterdienst, Zentralamt: Offenbach am Main.

Duveiller, G., Forzieri, G., Robertson, E., Li, W., Georgievski, G., Lawrence, P., et al. (2018). Biophysics and vegetation cover change: A process-based evaluation framework for confronting land surface models with satellite observations. *Earth System Science Data*, *10*(3), 1265–1279. https://doi.org/10.5194/essd-10-1265-2018

Duveiller, G., Hooker, J., & Cescatti, A. (2018). The mark of vegetation change on Earth's surface energy balance. *Nature Communications*, *9*(1), 679. https://doi.org/10.1038/s41467-017-02810-8

European Environmental Agency (2013). CORINE Land Cover (CLC) 2006, CRC/TR32 Database (TR32DB). Version 17. Copenhagen, Denmark: Copernicus Land Monitoring Service. Retrieved from https://www.eea.europa.eu/data-and-maps/data/clc-2006-raster-3

Ferguson, C. R., & Wood, E. F. (2011). Observed land–atmosphere coupling from satellite remote sensing and reanalysis. *Journal of Hydrometeorology*, *12*(6), 1221–1254. https://doi.org/10.1175/2011JHM1380.1

Findell, K. L., Berg, A., Gentine, P., Krasting, J. P., Lintner, B. R., Malyshev, S., et al. (2017). The impact of anthropogenic land use and land cover change on regional climate extremes. *Nature Communications*, *8*(1), 989. https://doi.org/10.1038/s41467-017-01038-w

Findell, K. L., & Eltahir, E. A. B. (2003a). Atmospheric controls on soil moisture–boundary layer interactions. Part I: Framework development. *Journal of Hydrometeorology*, *4*(3), 552–569. https://doi.org/10.1175/1525-7541(2003)004<0552:ACOSML>2.0.CO;2

Findell, K. L., & Eltahir, E. A. B. (2003b). Atmospheric controls on soil moisture–boundary layer interactions. Part II: Feedbacks within the continental United States. *Journal of Hydrometeorology*, *4*(3), 570–583. https://doi.org/10.1175/1525-7541(2003)004<0570:ACOSML>2.0.CO;2

Findell, K. L., Gentine, P., Lintner, B. R., & Kerr, C. (2011). Probability of afternoon precipitation in eastern United States and Mexico enhanced by high evaporation. *Nature Geoscience*, *4*(7), 434–439. https://doi.org/10.1038/ngeo1174

Gálos, B., Hagemann, S., Hänsler, A., Kindermann, G., Rechid, D., Sieck, K., et al. (2013). Case study for the assessment of the biogeophysical effects of a potential afforestation in Europe. *Carbon Balance and Management*, *8*(1), 3. https://doi.org/10.1186/1750-0680-8-3

Gao, Y., Markkanen, T., Backman, L., Henttonen, H. M., Pietikäinen, J.-P., Mäkelä, H. M., & Laaksonen, A. (2014). Biogeophysical impacts of peatland forestation on regional climate changes in Finland. *Biogeosciences*, *11*(24), 7251–7267. https://doi.org/10.5194/bg-11-7251-2014

Giorgi, F., Jones, C., & Asrar, G. R. (2009). Addressing climate information needs at the regional level: The CORDEX framework. *WMO Bulletin*, *58*(3).

Görsdorf, U., & Seifert, A. (2011). *Wolkenstatistik und Modellvalidierung auf der Basis kontinuierlicher Messungen eines 35 GHz-Radars (MOL-RAO Aktuell No. 1/2011)* (p. 2). Offenbach: DWD, Meteorologisches Observatorium Lindenberg - Richard-Aßmann-Observatorium. Retrieved from https://www.dwd.de/DE/forschung/atmosphaerenbeob/lindenbergersaeule/rao_download/aktuell_2011_01.pdf;jsessionid=138D9E89AD7372994E70DA92858AB197.live11041?__blob=publicationFile&v=5

Guillod, B. P., Orlowsky, B., Miralles, D. G., Teuling, A. J., & Seneviratne, S. I. (2015). Reconciling spatial and temporal soil moisture effects on afternoon rainfall. *Nature Communications*, *6*, 6443. https://doi.org/10.1038/ncomms7443

Guo, Z., & Dirmeyer, P. A. (2013). Interannual variability of land–atmosphere coupling strength. *Journal of Hydrometeorology*, *14*(5), 1636–1646. https://doi.org/10.1175/JHM-D-12-0171.1

Gutowski, W. J. Jr., Giorgi, F., Timbal, B., Frigon, A., Jacob, D., Kang, H.-S., et al. (2016). WCRP COordinated Regional Downscaling EXperiment (CORDEX): A diagnostic MIP for CMIP6. *Geoscientific Model Development*, *9*(11), 4087–4095. https://doi.org/10.5194/gmd-9-4087-2016

Hirsch, A. L., Pitman, A. J., Kala, J., Lorenz, R., & Donat, M. G. (2015). Modulation of land-use change impacts on temperature extremes via land–atmosphere coupling over Australia. *Earth Interactions*, *19*(12), 1–24. https://doi.org/10.1175/EI-D-15-0011.1

Huang, B., Hu, X., Fuglstad, G.-A., Zhou, X., Zhao, W., & Cherubini, F. (2020). Predominant regional biophysical cooling from recent land cover changes in Europe. *Nature Communications*, *11*(1), 1066. https://doi.org/10.1038/s41467-020-14890-0

Iacono, M. J., Delamere, J. S., Mlawer, E. J., Shephard, M. W., Clough, S. A., & Collins, W. D. (2008). Radiative forcing by long-lived greenhouse gases: Calculations with the AER radiative transfer models. *Journal of Geophysical Research*, *113*, D13103 https://doi.org/10.1029/2008JD009944

Ingwersen, J., Högy, P., Wizemann, H. D., Warrach-Sagi, K., & Streck, T. (2018). Coupling the land surface model Noah-MP with the generic crop growth model Gecros: Model description, calibration and validation. *Agricultural and Forest Meteorology*, *262*, 322–339. https://doi.org/10.1016/j.agrformet.2018.06.023

Intergovernmental Panel on Climate Change (Ed.) (2014). Anthropogenic and natural radiative forcing. In *Climate Change 2013 - the Physical Science Basis* (pp. 659–740). Cambridge: Cambridge University Press. https://doi.org/10.1017/CBO9781107415324.018

Intergovernmental Panel on Climate Change (2019). Climate Change and Land. Retrieved October 11, 2019, from https://www.ipcc.ch/report/srccl/

Jacob, D., Teichmann, C., Sobolowski, S., Katragkou, E., Anders, I., Belda, M., et al. (2020). Regional climate downscaling over Europe: Perspectives from the EURO-CORDEX community. *Regional Climate Change*, *20*(2), 1–20. https://doi.org/10.1007/s10113-020-01606-9

Kain, J. S. (2004). The Kain–Fritsch convective parameterization: An update. *Journal of Applied Meteorology*, *43*(1), 170–181. https://doi.org/10.1175/1520-0450(2004)043<0170:TKCPAU>2.0.CO;2

Knist, S., Goergen, K., Buonomo, E., Christensen, O. B., Colette, A., Cardoso, R. M., et al. (2017). Land-atmosphere coupling in EURO-CORDEX evaluation experiments: Land-atmosphere coupling in EURO-CORDEX. *Journal of Geophysical Research: Atmospheres*, *122*, 79–103. https://doi.org/10.1002/2016JD025476

Koster, R. D., Dirmeyer, P., Guo, Z., Bonan, G., Chan, E., Cox, P., et al. (2004). Regions of strong coupling between soil moisture and precipitation. *Science*, *305*(5687), 1138–1140. https://doi.org/10.1126/science.1100217

Kotlarski, S., Keuler, K., Christensen, O. B., Colette, A., Déqué, M., Gobiet, A., et al. (2014). Regional climate modeling on European scales: A joint standard evaluation of the EURO-CORDEX RCM ensemble. *Geoscientific Model Development*, *7*(4), 1297–1333. https://doi.org/10.5194/gmd-7-1297-2014

Kumar, S., Dirmeyer, P. A., Merwade, V., DelSole, T., Adams, J. M., & Niyogi, D. (2013). Land use/cover change impacts in CMIP5 climate simulations: A new methodology and 21st century challenges: LU CHANGE IMPACTS IN CMIP5. *Journal of Geophysical Research: Atmospheres*, *118*, 6337–6353. https://doi.org/10.1002/jgrd.50463

Lang, J. (2010). *Bericht zur Untersuchung konvektiver Wetterlagen in Nordrhein-Westfalen (Dokumentation des Projektes "konvektive Wetterlagen (KonWet)" No. 1)* (p. 25). Darmstadt, Germany: Landesamt für Natur, Umwelt und Verbraucherschutz Nordrhein-Westfalen.

Lawrence, P. J., & Chase, T. N. (2007). Representing a new MODIS consistent land surface in the Community Land Model (CLM 3.0). *Journal of Geophysical Research*, *112*, G01023. https://doi.org/10.1029/2006JG000168

Lawrence, P. J., & Chase, T. N. (2010). Investigating the climate impacts of global land cover change in the community climate system model. *International Journal of Climatology*, *30*(13), 2066–2087. https://doi.org/10.1002/joc.2061

Lejeune, Q., Seneviratne, S. I., & Davin, E. L. (2017). Historical land-cover change impacts on climate: Comparative assessment of LUCID and CMIP5 multimodel experiments. *Journal of Climate*, *30*(4), 1439–1459. https://doi.org/10.1175/JCLI-D-16-0213.1

Mahmood, R., Pielke, R. A., Hubbard, K. G., Niyogi, D., Dirmeyer, P. A., McAlpine, C., et al. (2014). Land cover changes and their biogeophysical effects on climate: Land cover changes and their biogeophysical effects on climate. *International Journal of Climatology*, *34*(4), 929–953. https://doi.org/10.1002/joc.3736

Milovac, J., Ingwersen, J., & Warrach-Sagi, K. (2014). *Soil texture forcing data for the whole world for the weather research and forecasting (WRF) model of the University of Hohenheim (UHOH) based on the harmonized world soil database (HWSD) at 30 arc-second horizontal resolution [data set]*. DKRZ, Hamburg, Germany: World Data Center for Climate (WDCC). https://doi.org/10.1594/WDCC/WRF_NOAH_HWSD_world_TOP_SOILTYP

Milovac, J., Warrach-Sagi, K., Behrendt, A., Späth, F., Ingwersen, J., & Wulfmeyer, V. (2016). Investigation of PBL schemes combining the WRF model simulations with scanning water vapor differential absorption lidar measurements: WRF sensitivity to PBL schemes and LSMs. *Journal of Geophysical Research: Atmospheres*, *121*, 624–649. https://doi.org/10.1002/2015JD023927

Nakanishi, M., & Niino, H. (2009). Development of an improved turbulence closure model for the atmospheric boundary layer. *Journal of the Meteorological Society of Japan*, *87*(5), 895–912. https://doi.org/10.2151/jmsj.87.895

Niu, G.-Y., Yang, Z.-L., Mitchell, K. E., Chen, F., Ek, M. B., Barlage, M., et al. (2011). The community Noah land surface model with multiparameterization options (Noah-MP): 1. Model description and evaluation with local-scale measurements. *Journal of Geophysical Research*, *116*, D12109. https://doi.org/10.1029/2010JD015139

Peel, M. C., Finlayson, B. L., & McMahon, T. A. (2007). Updated world map of the Köppen-Geiger climate classification. *Hydrology and Earth System Sciences*, *11*(5), 1633–1644. https://doi.org/10.5194/hess-11-1633-2007

Pfahl, S., & Wernli, H. (2012). Quantifying the relevance of cyclones for precipitation extremes. *Journal of Climate*, *25*(19), 6770–6780. https://doi.org/10.1175/JCLI-D-11-00705.1

Pitman, A. J., de Noblet-Ducoudré, N., Cruz, F. T., Davin, E. L., Bonan, G. B., Brovkin, V., et al. (2009). Uncertainties in climate responses to past land cover change: First results from the LUCID intercomparison study. *Geophysical Research Letters*, *36*, L14814. https://doi.org/10.1029/2009GL039076

Rechid, D., Davin, E. L., de Noblet-Ducoudré, N., Katragkou, E., & LUCAS-Team (2017). CORDEX Flagship Pilot Study LUCAS—Land Use & Climate Across Scales—A new initiative on coordinated regional land use change and climate experiments for Europe. In *Presented at the 19th EGU General Assembly, EGU2017* (Vol. 19, p. 13172). Vienna, Austria: Geophysical Research Abstracts.

Santanello, J. A., Peters-Lidard, C. D., Kumar, S. V., Alonge, C., & Tao, W.-K. (2009). A modeling and observational framework for diagnosing local land–atmosphere coupling on diurnal time scales. *Journal of Hydrometeorology*, *10*(3), 577–599. https://doi.org/10.1175/2009JHM1066.1

Schwitalla, T., Bauer, H.-S., Wulfmeyer, V., & Warrach-Sagi, K. (2017). Continuous high-resolution midlatitude-belt simulations for July–August 2013 with WRF. *Geoscientific Model Development*, *10*(5), 2031–2055. https://doi.org/10.5194/gmd-10-2031-2017

Seneviratne, S. I., Lüthi, D., Litschi, M., & Schär, C. (2006). Land–atmosphere coupling and climate change in Europe. *Nature*, *443*(7108), 205–209. https://doi.org/10.1038/nature05095

Seneviratne, S. I., Wilhelm, M., Stanelle, T., Hurk, B., Hagemann, S., Berg, A., et al. (2013). Impact of soil moisture-climate feedbacks on CMIP5 projections: First results from the GLACE-CMIP5 experiment. *Geophysical Research Letters*, *40*(19), 5212–5217. https://doi.org/10.1002/grl.50956

Skamarock, W., Klemp, J., Dudhia, J., Gill, D., Barker, D., Wang, W., et al. (2008). *A description of the advanced research WRF version 3*. Boulder, CO: UCAR/NCAR. https://doi.org/10.5065/D68S4MVH

Snyder, P. K., Delire, C., & Foley, J. A. (2004). Evaluating the influence of different vegetation biomes on the global climate. *Climate Dynamics*, *23*(3–4), 279–302. https://doi.org/10.1007/s00382-004-0430-0

Späth, F., Wulfmeyer, V., Streck, T., & Behrendt, A. (2019). *The Land-Atmosphere Feedback Observatory (LAFO): A Novel Sensor Network to Improve Weather Forecasting and Climate Models. Presented at the EGU General Assembly*. Vienna, Austria: Geophysical Research Abstracts.

Strandberg, G., & Kjellström, E. (2019). Climate impacts from afforestation and deforestation in Europe. *Earth Interactions*, *23*(1), 1–27. https://doi.org/10.1175/EI-D-17-0033.1

Taylor, C. M., de Jeu, R. A. M., Guichard, F., Harris, P. P., & Dorigo, W. A. (2012). Afternoon rain more likely over drier soils. *Nature*, *489*(7416), 423–426. https://doi.org/10.1038/nature11377

Thompson, G., Rasmussen, R. M., & Manning, K. (2004). Explicit forecasts of winter precipitation using an improved bulk microphysics scheme. Part I: Description and sensitivity analysis. *Monthly Weather Review*, *132*(2), 519–542. https://doi.org/10.1175/1520-0493(2004)132<0519:EFOWPU>2.0.CO;2

Tölle, M. H., Gutjahr, O., Busch, G., & Thiele, J. C. (2014). Increasing bioenergy production on arable land: Does the regional and local climate respond? Germany as a case study. *Journal of Geophysical Research: Atmospheres*, *119*, 2711–2724. https://doi.org/10.1002/2013JD020877

van den Hurk, B. J. J. M., & van Meijgaard, E. (2010). Diagnosing land–atmosphere interaction from a regional climate model simulation over West Africa. *Journal of Hydrometeorology*, *11*(2), 467–481. https://doi.org/10.1175/2009JHM1173.1

Warrach-Sagi, K., Schwitalla, T., Wulfmeyer, V., & Bauer, H.-S. (2013). Evaluation of a climate simulation in Europe based on the WRF–NOAH model system: Precipitation in Germany. *Climate Dynamics*, *41*(3–4), 755–774. https://doi.org/10.1007/s00382-013-1727-7

Winckler, J., Reick, C. H., & Pongratz, J. (2017). Robust identification of local biogeophysical effects of land-cover change in a global climate model. *Journal of Climate*, *30*(3), 1159–1176. https://doi.org/10.1175/JCLI-D-16-0067.1

Wulfmeyer, V., Späth, F., Behrendt, A., Jach, L., Warrach-Sagi, K., Ek, M., et al. (2020). The GEWEX Land-Atmosphere Feedback Observatory (GLAFO). *GEWEX Quarterly Newsletter*, *30*(1/2020), 16. https://www.gewex.org/gewex-content/files_mf/1583952472Feb2020.pdf

Wulfmeyer, V., Turner, D. D., Baker, B., Banta, R., Behrendt, A., Bonin, T., et al. (2018). A new research approach for observing and characterizing land–atmosphere feedback. *Bulletin of the American Meteorological Society*, *99*(8), 1639–1667. https://doi.org/10.1175/BAMS-D-17-0009.1